

# SU( $N$ ) Kondo-Heisenberg chain: Phase diagram, Ising criticality, and the coexistence of heavy quasiparticles and valence bond solid order

Marcin Raczkowski<sup>1</sup> and Fakher F. Assaad<sup>2</sup>

<sup>1</sup>*Institut für Theoretische Physik und Astrophysik,  
Universität Würzburg, 97074 Würzburg, Germany*

<sup>2</sup>*Institut für Theoretische Physik und Astrophysik and Würzburg-Dresden Cluster of Excellence ct.qmat,  
Universität Würzburg, 97074 Würzburg, Germany*

(Dated: May 24, 2024)

We map out the ground state phase diagram of a one-dimensional SU( $N$ ) Kondo-Heisenberg lattice model at half filling and in the fully antisymmetric self-adjoint representation as a function of  $\frac{1}{N}$  and Kondo coupling  $J_k/t$ . On the basis of auxiliary field quantum Monte Carlo (QMC) simulations with even  $N$  up to 8, we show that the enlarged SU( $N \geq 4$ ) symmetry realizes a quantum phase transition separating a valence bond solid (VBS) phase occupying a weak coupling part of the phase diagram and the Kondo insulator (KI) state dominating in the strong  $J_k/t$  limit. Along the phase boundary, we always observe critical exponents that belong to a two-dimensional classical Ising universality class. We next trace the evolution of the composite fermion and spin spectral functions across the phase boundary and conclude that VBS order triggers a bond order wave state of conduction electrons, both coexisting with Kondo screening. Upon further reducing  $J_k/t$  we observe that composite quasiparticles lose their spectral weight indicating that VBS order gradually liberates localized  $f$  spins from forming Kondo singlets with conduction electron spins. We contrast the QMC results with a static large- $N$  approximation, and we show that in the limit of infinite degeneracy  $N \rightarrow \infty$  the order-disorder transition becomes of first order and is accompanied by a full decoupling of conduction electrons and localized  $f$  spins. We complete our analysis by considering the limit of a vanishing Heisenberg coupling  $J_h = 0$ , and we provide evidence that the enlarged SU( $N$ ) symmetry and low dimensionality of the RKKY exchange interaction are not sufficient to induce VBS order in the conventional SU( $N$ ) Kondo chain which hosts solely a KI phase. Finally, we quantify the role of increasing  $N$  in reducing the separation of charge and spin times scales specific to the KI state, and we show that the latter is adiabatically connected to a trivial band insulator captured by the large- $N$  approximation.

## I. INTRODUCTION

The complexity of solving the Kondo lattice model arises from many body correlation effects involving both the localized spin and the itinerant electron degrees of freedom [1]. A coherent Bloch-like screening of impurity spins by conduction electrons leads to the formation of a heavy Fermi liquid state [2–5]. The volume of the resultant large Fermi surface includes both the localized spins and conduction electrons [6]. Depending on the strength of Kondo coupling  $J_k/t$ , the Kondo quenching might be incomplete or even gets broken down by the competing Rudermann-Kittel-Kasuya-Yosida (RKKY) interaction. The latter corresponds to an indirect coupling between magnetic impurities mediated by the conduction electrons and promotes a magnetically ordered state. The breakdown of the Kondo effect [7–11] or equivalently the orbital selective Mott transition [12–14] involves a reconstruction of the Fermi surface such that its volume is determined solely by the conduction electrons.

These two underlying physical mechanisms, lattice Kondo screening and RKKY interaction, are believed to determine the physical properties of heavy fermion compounds with  $f$  electron orbitals [15–17]. Following a phenomenological approach by Doniach [1], substantial analytical and numerical efforts have been undertaken to deepen our understanding of a resultant magnetic order-

disorder transition in a two-dimensional (2D) Kondo lattice model [18–37].

While long range antiferromagnetic order does not appear in a strictly one-dimensional (1D) geometry, the physics of a dense Kondo chain at half filling turns out to be equally exciting. While a semiclassical analysis based on the nonlinear  $\sigma$  model [38], bosonization approach [39], exact diagonalization [40], and density-matrix renormalization group (DMRG) calculations [41] yield an exponentially small spin excitation gap, the charge gap was shown to track  $J_k$  for small Kondo couplings instead [41, 42]. Thus strong antiferromagnetic spin correlations in a Kondo insulator lead to the separation of spin and charge energy scales [43–46] absent in a trivial band insulator [47, 48]. The precise nature of the spin excitation spectrum in a Kondo insulator has been the subject of recent debate [49, 50]. Furthermore, a generalized Luttinger theorem guarantees that, in a translationally invariant case, the large filled Fermi sea picture holds for an arbitrarily small value of  $J_k/t$  [51]. Tracing spectral signatures of the heavy Tomonaga-Luttinger liquid constitutes, however, an ongoing challenge for numerical simulations carried out on finite size systems [52–60].

In comparison, much less is known about the occurrence of dimer order in the Kondo lattice model beyond the static large- $N$  approximation [61–66]. A frequently used route to address numerically the interplay

of dimerization and Kondo screening is to include geometrical frustration [67]. For example, DMRG studies of a Kondo lattice model on the zigzag ladder discovered a spontaneous dimerization as an easy way out to alleviate the magnetic frustration [68–70]. Another possibility is to consider a spin-1/2 Heisenberg 1D chain with competing nearest- and next-nearest-neighbor interactions  $J_h$  and  $J'_h$ , respectively, tuned to the dimerized Majumdar-Ghosh point [71, 72] and to explore the fate of the spin-dimerized phase when Kondo-coupled to the Fermi sea [73–75].

A key idea of this paper is to consider a generalized Kondo-Heisenberg chain characterized by a spin symmetry group extended from  $SU(2)$  to  $SU(N)$ . On the one hand, it is known that already an  $SU(4)$  Heisenberg chain has a dimerized ground state [76, 77]. The two-fold degeneracy of the latter comes from two choices of forming a singlet dimer with either a left or right nearest neighbor spin. On the other hand, the ground state of the  $SU(4)$  Kondo-Heisenberg model in the strong Kondo coupling  $J_k/J_h \rightarrow \infty$  shall be given by a direct product of Kondo singlets. Thus, it is plausible that increasing Kondo coupling  $J_k/t$  in the  $SU(4)$  Kondo-Heisenberg chain will drive a phase transition from a dimerized ground state to the Kondo insulating phase. Since both phases possess a finite spin gap, one can assume that the essential dynamics of the model is dominated by short range valence bond configurations and the problem should be effectively captured by an Ising gauge theory, known to be dual to the 1D transverse field Ising model [78]. Thus based on quantum-classical mapping, we foresee that the phase transition belongs to the 2D classical Ising universality class.

A related issue concerns the existence of a spontaneously dimerized state of the localized spins driven solely by the RKKY interaction. On the one hand, our detailed study of the phase diagram and the low energy properties of the 2D  $SU(N)$  Kondo lattice model in the fully antisymmetric self-adjoint representation led us to conclude that no other phases aside from the Kondo insulator and Néel state intervene at half filling [35]. On the other hand, early DMRG evidence of an insulating dimerized ground state in the weak-coupling regime  $J_k/t \lesssim 1.2$  of the quarter-filled 1D Kondo lattice model [79, 80] has recently been confirmed, along with the coexisting bond order wave state of conduction electrons, by unbiased infinite DMRG calculations [81]. Hence, the low dimensionality of the RKKY interaction could possibly enhance dimer fluctuations thus motivating studies of a pure  $SU(N)$  Kondo chain as well.

In fact, quantum simulations with alkali-earth-like atoms in optical lattices have already made the  $SU(N)$  quantum magnetism tangible [82]. Steady progress in this domain allows one to envisage a highly controllable implementation of the Kondo singlet state with an enlarged  $SU(N)$  symmetry in single impurity and lattice situations in the near future [83–86].

In addition to a general interest in exploring novel

quantum many-body phenomena driven by  $SU(N)$  symmetric interactions in low dimensions, an additional motivation to study 1D Kondo chains is provided by real materials, e.g., a recently discovered Kondo lattice compound  $CeCo_2Ga_8$  [87]. Upon cooling, resistivity measurements [88] and optical spectra [89] of  $CeCo_2Ga_8$  indicate the occurrence of coherent Kondo screening along one single crystal direction. Thus,  $CeCo_2Ga_8$  represents a rare example of quasi-1D heavy fermion behavior and numerical results obtained in the 1D geometry can serve as a starting point to develop at least qualitatively theories of such a state.

The rest of the paper is organized as follows. In Sec. II we introduce an  $SU(N)$  Kondo-Heisenberg Hamiltonian, we discuss its mapping onto the  $U(1)$  lattice gauge theory which sets the basis for our auxiliary field quantum Monte Carlo (QMC) simulations, and we describe the saddle-point approximation to the auxiliary field action. Next, we present an extended discussion of the numerical results by considering in Sec. III A the  $SU(N)$  Kondo-Heisenberg model and in Sec. III B a pure  $SU(N)$  Kondo chain. Finally, Sec. IV gives a summary and outlook.

## II. MODEL AND METHODS

Here we first define the model. We then use a numerically exact approach, quantum Monte Carlo (QMC), to solve the problem. In the presence of particle-hole symmetry this approach can be formulated without confronting the so-called negative sign problem such that we can obtain numerically exact zero temperature results with computational costs scaling as the cube of the number of lattice sites times the so-called projection parameter  $\Theta$ . Since the particle-hole symmetry is not broken for even values of fermion flavors  $N$ , this method can also be used, at no extra computational cost, for the  $SU(N)$  model. The limitations occur at finite doping where we encounter the negative sign problem and an exponential scaling of the computational costs with lattice size. We will compare our results with large- $N$  mean-field theories. Strictly speaking these methods are not controlled, and they can produce wrong results, if e.g. there is a phase transition between the finite  $N$  case of interest and  $N = \infty$ .

### A. Model

The Kondo-Heisenberg chain Hamiltonian reads [90–95]:

$$\hat{H} = \hat{H}_t + \hat{H}_{J_k} + \hat{H}_{J_h}, \quad (1)$$

$$\hat{H}_t = -t \sum_{\langle i,j \rangle} (\hat{c}_i^\dagger \hat{c}_j + h.c.), \quad (2)$$

$$\hat{H}_{J_k} = \frac{J_k}{2} \sum_{i=1}^L \hat{c}_i^\dagger \boldsymbol{\sigma} \hat{c}_i \cdot \hat{\mathbf{S}}_i, \quad (3)$$

$$\hat{H}_{J_h} = J_h \sum_{i=1}^L \hat{\mathbf{S}}_i \cdot \hat{\mathbf{S}}_{i+1}, \quad (4)$$

where  $\hat{c}_i^\dagger = (\hat{c}_{i,\uparrow}^\dagger, \hat{c}_{i,\downarrow}^\dagger)$  is a spinor where  $\hat{c}_{i,\sigma}^\dagger$  creates an electron in Wannier state centered around lattice site  $i$  and  $z$  component of spin  $\sigma = \uparrow, \downarrow$ ;  $t$  is the nearest-neighbor hopping amplitude,  $J_k$  is the Kondo exchange coupling between the spins of conduction electrons and the localized spin  $s = 1/2$  degrees of freedom,  $\hat{\mathbf{S}}_i$ , with  $\boldsymbol{\sigma}$  being a vector of Pauli spin matrices,  $J_h$  is the nearest-neighbor Heisenberg exchange interaction, and  $L$  is the length of the chain.

To incorporate a general flavor symmetry  $SU(N)$ , we generalize the above model with the help of a fermionic representation of the  $SU(N)$  generators,

$$\hat{S}_{i,\nu}^\mu = \hat{f}_{i,\nu}^\dagger \hat{f}_{i,\mu} - \frac{\delta_{\mu,\nu}}{N} \sum_{\sigma=1}^N \hat{f}_{i,\sigma}^\dagger \hat{f}_{i,\sigma}, \quad (5)$$

subject to the local constraint,

$$\sum_{\sigma=1}^N \hat{f}_{i,\sigma}^\dagger \hat{f}_{i,\sigma} = \frac{N}{2}. \quad (6)$$

It selects the fully antisymmetric self-adjoint representation corresponding to a Young tableau with a single column and  $N/2$  rows [35, 96, 97].

### B. QMC formulation

In the above representation, the model Eq. (1) reads,

$$\begin{aligned} \hat{H} = & \hat{H}_t - \frac{J_k}{4N} \sum_i \left\{ (\hat{c}_i^\dagger \hat{\mathbf{f}}_i + h.c.)^2 + (i \hat{c}_i^\dagger \hat{\mathbf{f}}_i + h.c.)^2 \right\} \\ & - \frac{J_h}{4N} \sum_i \left\{ (\hat{\mathbf{f}}_i \hat{\mathbf{f}}_{i+1} + h.c.)^2 + (i \hat{\mathbf{f}}_i \hat{\mathbf{f}}_{i+1} + h.c.)^2 \right\} \\ & + \frac{U}{N} \sum_i \left( \hat{\mathbf{f}}_i \hat{\mathbf{f}}_i - \frac{N}{2} \right)^2, \end{aligned} \quad (7)$$

where  $\hat{c}_i^\dagger$  and  $\hat{\mathbf{f}}_i^\dagger$  are both  $N$  flavor spinor operators. Note that the extra Hubbard- $U$  interaction term commutes with the Hamiltonian and suppresses charge fluctuations on the  $f$  orbitals by the Boltzmann factor  $\propto e^{-\Theta U/N}$ . This guarantees that the constraint Eq. (6) will be automatically imposed in simulations with any finite positive  $U$  and when the projection parameter  $\Theta$  is chosen to be sufficiently large.

To proceed we use the Trotter decomposition and Hubbard Stratonovich transformation to decouple the perfect square terms in Eq. (7). To this end, we introduce complex bond fields  $\mathcal{V}(\mathbf{i}, \tau)$  and  $\chi(\mathbf{i}, \tau)$  to handle the dynamics of Kondo and Heisenberg terms as well as the scalar Lagrange multiplier  $\lambda(\mathbf{i}, \tau)$  to enforce the constraint. Since all the three fields couple to  $SU(N)$  symmetric operators, the number of flavors  $N$  can be pulled out in front of the action and one arrives at the following form for the grand-canonical partition function

$$Z \equiv \int \mathcal{D}\{\mathcal{V}, \chi, \lambda\} e^{-N\mathcal{S}\{\mathcal{V}, \chi, \lambda\}} \quad (8)$$

with the action

$$\begin{aligned} \mathcal{S}\{\mathcal{V}, \chi, \lambda\} = & -\ln \left[ \text{Tr} \mathcal{T} e^{-\int_0^\beta d\tau \hat{H}\{\mathcal{V}, \chi, \lambda\}} \right] \\ & + \int_0^\beta d\tau \sum_i \left\{ \frac{J_k}{4} |\mathcal{V}(\mathbf{i}, \tau)|^2 \right. \\ & \left. + \frac{J_h}{4} |\chi(\mathbf{i}, \tau)|^2 + \frac{U}{4} |\lambda(\mathbf{i}, \tau)|^2 \right\} \end{aligned} \quad (9)$$

and the time dependent Hamiltonian

$$\hat{H}\{\mathcal{V}, \chi, \lambda\} = \hat{H}_t + \sum_{\mathbf{i}} \left\{ -\frac{J_k}{2} \left( \mathcal{V}(\mathbf{i}, \tau) \hat{c}_{\mathbf{i}}^\dagger \hat{f}_{\mathbf{i}} + h.c. \right) - \frac{J_h}{2} \left( \chi(\mathbf{i}, \tau) \hat{f}_{\mathbf{i}}^\dagger \hat{f}_{\mathbf{i}+1} + h.c. \right) - iU\lambda(\mathbf{i}, \tau) \left( \hat{f}_{\mathbf{i}}^\dagger \hat{f}_{\mathbf{i}} - \frac{1}{2} \right) \right\}. \quad (10)$$

Note that in the above the spinor operators  $\hat{c}_{\mathbf{i}}^\dagger$  and  $\hat{f}_{\mathbf{i}}^\dagger$  have lost their flavor index  $N$  since it merely comes in to Eq. (8) as a parameter.

As a matter of fact, by using Grassmann variables [98]  $\mathbf{c}(\mathbf{i}, \tau)$  and  $\mathbf{f}(\mathbf{i}, \tau)$  and taking the limit  $U \rightarrow \infty$ , one can show that the constraint leads to a local U(1) gauge invariance of the action [10, 99–101]. In that case, the canonical transformation,  $\mathbf{f}(\mathbf{i}, \tau) \rightarrow e^{i\varphi_{\mathbf{i}}(\tau)} \mathbf{f}(\mathbf{i}, \tau)$  amounts to redefining the fields  $\mathcal{V}(\mathbf{i}, \tau) \rightarrow e^{-i\varphi_{\mathbf{i}}(\tau)} \mathcal{V}(\mathbf{i}, \tau)$ ,  $\chi(\mathbf{i}, \tau) \rightarrow e^{i\varphi_{\mathbf{i}}(\tau)} \chi(\mathbf{i}, \tau) e^{-i\varphi_{\mathbf{i}+1}(\tau)}$ , and  $\lambda(\mathbf{i}, \tau) \rightarrow \lambda(\mathbf{i}, \tau) + \partial_\tau \varphi_{\mathbf{i}}(\tau)$ , such that the partition function remains invariant. As is apparent, fermion fields  $\mathbf{f}(\mathbf{i}, \tau)$  carry the unit gauge charge. It is, however, possible to define a gauge neutral field

$$\tilde{\mathbf{f}}(\mathbf{i}, \tau) = e^{i\varphi_{\mathbf{i}}(\tau)} \mathbf{f}(\mathbf{i}, \tau), \quad \text{with } e^{i\varphi_{\mathbf{i}}(\tau)} = \frac{\mathcal{V}(\mathbf{i}, \tau)}{|\mathcal{V}(\mathbf{i}, \tau)|} \quad (11)$$

which has quantum numbers of a physical fermion. In the heavy fermion phase,  $\tilde{\mathbf{f}}(\mathbf{i}, \tau)$  emerges then as a new particle excitation that acquires coherence and contributes to the Luttinger volume.

The above can be understood in terms of a Higgs [102] mechanism in which the phase fluctuations of  $\varphi_{\mathbf{i}}(\tau)$  become very slow such that  $\varphi_{\mathbf{i}}(\tau)$  can be set to a constant. In this case there is no distinction between the fields  $\tilde{\mathbf{f}}(\mathbf{i}, \tau)$  and  $\mathbf{f}(\mathbf{i}, \tau)$  or, in other words,  $\mathbf{f}(\mathbf{i}, \tau)$  has lost its gauge charge and has acquired a unit electric charge. This Higgs mechanism is captured in mean-field large- $N$  approaches of the Kondo lattice where Kondo screening corresponds to  $\langle \mathcal{V}(\mathbf{i}, \tau) \rangle \neq 0$  [103, 104]. Moreover, as shown in Ref. [36] and in the large- $N$  limit,  $\tilde{\mathbf{f}}(\mathbf{i}, \tau)$  is nothing but the so-called composite fermion field [105, 106]:

$$\tilde{\mathbf{f}}(\mathbf{i}, \tau) \propto \boldsymbol{\psi}(\mathbf{i}, \tau) = \mathbf{S}(\mathbf{i}, \tau) \cdot \boldsymbol{\sigma} \mathbf{c}(\mathbf{i}, \tau). \quad (12)$$

More specifically, for Kondo impurity problems the Green's function of  $\hat{\boldsymbol{\psi}}_{\mathbf{i}}^\dagger$  corresponds to the  $T$ -matrix [107] while  $\hat{\boldsymbol{\psi}}_{\mathbf{i}}^\dagger$  itself corresponds to the Schrieffer-Wolff transformation of the localized electron operator in the realm of the Anderson model [3].

The mapping of the model Eq. (7) onto the U(1) lattice gauge theory sets the basis for our auxiliary field QMC simulations [108–110]. The integration over the Grassmann variables yields the fermion determinant which, for a particle-hole symmetric conduction electron band and even values of  $N$  used in our study, is positive semi-definite such that no negative sign problem occurs [111]. The integration over the Hubbard-Stratonovich fields is then conveniently carried out with Monte Carlo importance sampling. Specifically for the calculation presented here, we have used the implementation of the Kondo lat-

tice model of the Algorithms for Lattice Fermions (ALF-2.0) library [112] extended by the Heisenberg term, and we adopted a projective (zero-temperature) version of the algorithm. It is based on the imaginary time evolution of a trial wave function  $|\Psi_T\rangle$ , with  $\langle \Psi_T | \Psi_0 \rangle \neq 0$ , to the ground state  $|\Psi_0\rangle$ :

$$\frac{\langle \Psi_0 | \hat{O} | \Psi_0 \rangle}{\langle \Psi_0 | \Psi_0 \rangle} = \lim_{\Theta \rightarrow \infty} \frac{\langle \Psi_T | e^{-\Theta \hat{H}} \hat{O} e^{-\Theta \hat{H}} | \Psi_T \rangle}{\langle \Psi_T | e^{-2\Theta \hat{H}} | \Psi_T \rangle}. \quad (13)$$

To assess the hermiticity of the imaginary time propagation in the presence of current operators in Eq. (7), we have opted for a symmetric Trotter decomposition [112] with a finite imaginary time step  $\Delta\tau t = 0.1$ . Furthermore, we used a  $J_k$  and  $N$  dependent projection parameter  $20 \leq 2\Theta t \leq 200$  chosen large enough to obtain converged ground-state quantities in test run simulations. As for the constraint, the choice  $2\Theta U/N \geq 10$  was found sufficient to suppress charge fluctuations on the  $f$  sites within statistical uncertainty. Finally, for the analytical continuation of the single and two particle imaginary time QMC data, we have made use of the stochastic maximum entropy method [113, 114] implemented in the ALF-2.0 library.

Let us emphasize that the formulation of the auxiliary field QMC approach maps the Kondo lattice model onto a compact U(1) lattice gauge theory, where the local U(1) symmetry reflects the infinitely strong bare coupling. The Monte Carlo simulations that we carry out make no approximations, and correspond to an exact integration over the gauge fields. By systematically carrying out simulations at larger and larger values of  $N$  we can actually assess, as was done in Ref. [35], that there is no phase transition between the  $N = 2$  Kondo insulating state and the one at  $N = \infty$  for the 2D case. This adiabatic path between  $N = 2$  and  $N = \infty$  is in our view an important numerical result that can justify the large- $N$  approximation, which we discuss in the next section.

### C. Large- $N$ approach

In the large- $N$  limit, the saddle-point approximation to the action Eq. (9):

$$\frac{\partial \mathcal{S}\{\mathcal{V}, \chi, \lambda\}}{\partial \mathcal{V}(\mathbf{i}, \tau)}, \quad \frac{\partial \mathcal{S}\{\mathcal{V}^*, \chi^*, \lambda\}}{\partial \mathcal{V}^*(\mathbf{i}, \tau)} = 0, \quad (14)$$

$$\frac{\partial \mathcal{S}\{\mathcal{V}, \chi, \lambda\}}{\partial \chi(\mathbf{i}, \tau)}, \quad \frac{\partial \mathcal{S}\{\mathcal{V}^*, \chi^*, \lambda\}}{\partial \chi^*(\mathbf{i}, \tau)} = 0, \quad \text{and} \quad (15)$$

$$\frac{\partial \mathcal{S}\{\mathcal{V}, \chi, \lambda\}}{\partial \lambda(\mathbf{i}, \tau)} = 0, \quad (16)$$

becomes exact. In the mean-field approximation carried out below, we consider only saddle points with time independent fields. We furthermore assume translational invariance of the field  $\mathcal{V}(\mathbf{i}, \tau) = \mathcal{V}^*(\mathbf{i}, \tau) = V(\in \mathbb{R})$ , introduced to handle the Kondo term, but since we are interested in a solution with dimer order and the resultant doubling of the unit cell, we allow for a site dependent field,  $\chi(\mathbf{i}, \tau) = \chi^*(\mathbf{i}, \tau) = \chi_{\mathbf{i}}(\in \mathbb{R})$ , used to decouple the Heisenberg term. Furthermore, since the 1D geometry of the Kondo-Heisenberg chain does not sustain solutions involving spontaneous breaking of a continuous spin rotational symmetry group, we leave out in our analysis long range antiferromagnetic order. Finally, in the large- $N$  approach, the constraint is enforced only on average by means of a Lagrange multiplier  $\lambda$ .

We perform a standard mean-field decoupling [101, 115, 116] based on the hybridization order parameter  $V = \langle \hat{f}_{\mathbf{i}}^{\dagger} \hat{c}_{\mathbf{i}} + h.c. \rangle$  measuring the strength of Kondo screening and the valence bond order parameter  $\chi_{\mathbf{i}} = \langle \hat{f}_{\mathbf{i}}^{\dagger} \hat{f}_{\mathbf{i}+\mathbf{1}} + h.c. \rangle$  accounting for a spinon description of the spin-1/2 Heisenberg antiferromagnetic chain [117, 118]. Given that the smallest unit cell capturing the valence bond solid (VBS) phase consists of two sites, we split the lattice into sublattices  $A$  and  $B$ , and assume a perfect dimerization of the chain,  $\chi_A = \chi_0 + \delta$  and  $\chi_B = \chi_0 - \delta$ , such that  $\chi_0 = \frac{1}{2}(\chi_A + \chi_B)$  [ $\delta = \frac{1}{2}(\chi_A - \chi_B)$ ] correspond to the uniform (staggered) part of the valence bond order parameter, respectively. Within the above Ansatz, the mean-field (MF) Hamiltonian takes the following Fourier transformed form:

$$\begin{aligned} \hat{H}_{MF} = & \sum_{\mathbf{k} \in RBZ} \left( \hat{c}_{\mathbf{k}}^{\dagger}, \hat{c}_{\mathbf{k}+\boldsymbol{\pi}}^{\dagger}, \hat{f}_{\mathbf{k}}^{\dagger}, \hat{f}_{\mathbf{k}+\boldsymbol{\pi}}^{\dagger} \right) \\ & \times \begin{pmatrix} \epsilon(\mathbf{k}) & 0 & -\frac{J_k V}{2} & 0 \\ 0 & -\epsilon(\mathbf{k}) & 0 & -\frac{J_k V}{2} \\ -\frac{J_k V}{2} & 0 & \epsilon_f(\mathbf{k}) & i\tilde{\epsilon}_f(\mathbf{k}) \\ 0 & -\frac{J_k V}{2} & -i\tilde{\epsilon}_f(\mathbf{k}) & -\epsilon_f(\mathbf{k}) \end{pmatrix} \\ & \times \begin{pmatrix} \hat{c}_{\mathbf{k}} \\ \hat{c}_{\mathbf{k}+\boldsymbol{\pi}} \\ \hat{f}_{\mathbf{k}} \\ \hat{f}_{\mathbf{k}+\boldsymbol{\pi}} \end{pmatrix} + \frac{N_u}{2} [J_h(\chi_0^2 + \delta^2) + J_k V^2], \quad (17) \end{aligned}$$

where  $\epsilon(\mathbf{k}) = -2t \cos k$  and  $\epsilon_f(\mathbf{k}) = -J_h \chi_0 \cos k$  such that  $\epsilon(\mathbf{k} + \boldsymbol{\pi}) = -\epsilon(\mathbf{k})$  and  $\epsilon_f(\mathbf{k} + \boldsymbol{\pi}) = -\epsilon_f(\mathbf{k})$ ;  $\tilde{\epsilon}_f(\mathbf{k}) = -J_h \delta \sin k$ , the  $\mathbf{k}$  sum runs over a reduced Brillouin zone (RBZ), and  $N_u$  denotes the number of unit cells. Note that since the underlying particle hole-symmetry pins automatically the  $f$  occupation to half filling, in the above we have left out the Lagrange multiplier  $\lambda$ . The saddle-point equations then read:

$$\frac{\partial F}{\partial \chi_0} = \frac{\partial F}{\partial \delta} = \frac{\partial F}{\partial V} = 0, \quad (18)$$

with  $F = -\frac{1}{\beta} \ln \text{Tr} e^{-\beta \hat{H}_{MF}}$ .

In principle, a spin dimerization on the  $f$  spin layer can trigger, via Kondo coupling  $J_k$ , a bond order wave

(BOW) state with a dimerized kinetic energy of the conduction electrons such that  $\xi_A \neq \xi_B$  where  $\xi_{\mathbf{i}} = \langle \hat{c}_{\mathbf{i}}^{\dagger} \hat{c}_{\mathbf{i}+\mathbf{1}} + h.c. \rangle$  [75, 81]. Before exploring this issue by numerically solving the saddle-point equations in Sec. III A 2, let us first discuss the following three limiting cases, each of them reducing the  $4 \times 4$  matrix in Eq. (17) to a  $2 \times 2$  matrix problem:

- Vanishing Heisenberg interaction  $J_h = 0$ , i.e., conventional Kondo chain with the RKKY energy scale being the only intersite exchange interaction between the localized  $f$  spins. Assuming a finite hybridization order parameter  $V \neq 0$  as appropriate for the KI phase, one arrives at the single particle dispersion relation,

$$E_{\mathbf{k}}^{\pm} = \frac{\epsilon(\mathbf{k}) \pm \sqrt{\epsilon^2(\mathbf{k}) + (J_k V)^2}}{2}, \quad (19)$$

and the corresponding quasiparticle residues

$$Z_{\mathbf{k}}^{f,c} = \frac{1}{2} \left[ 1 \pm \frac{\epsilon(\mathbf{k})}{\sqrt{\epsilon^2(\mathbf{k}) + (J_k V)^2}} \right], \quad (20)$$

with  $+$  ( $-$ ) sign denoting a doped hole away from half filling into the  $f$  ( $c$ ) state, respectively. As illustrated in Fig. 1, the resultant low energy hybridized bands are nearly dispersionless, extend up to  $\mathbf{k} = \pi$  momentum, and have predominantly  $f$  character. While decreasing  $J_k/t$  reduces both the slope of the hybridized bands and the  $c$  electron spectral weight at  $\mathbf{k} = \pi$ , the quasiparticle (QP) gap remains pinned to  $\mathbf{k} = \pi$ ,  $\Delta_{qp} \equiv \min_{\mathbf{k}} \Delta_{qp}(\mathbf{k}) = -E_{\mathbf{k}=\pi}^-$ .

- Vanishing dimerization order parameter  $\delta = 0$ ; consequently  $\tilde{\epsilon}_f(\mathbf{k}) = 0$  for each  $\mathbf{k}$ . The delocalization of spinons via  $\epsilon_f(\mathbf{k})$  on top of that through a finite hybridization order parameter  $V$  modifies the dispersion relation of the hybridized bands,

$$E_{\mathbf{k}}^{\pm} = \frac{\epsilon(\mathbf{k}) + \epsilon_f(\mathbf{k}) \pm \sqrt{[\epsilon(\mathbf{k}) - \epsilon_f(\mathbf{k})]^2 + (J_k V)^2}}{2}, \quad (21)$$

as well as the QP weights

$$Z_{\mathbf{k}}^{f,c} = \frac{1}{2} \left[ 1 \pm \frac{\epsilon(\mathbf{k}) - \epsilon_f(\mathbf{k})}{\sqrt{[\epsilon(\mathbf{k}) - \epsilon_f(\mathbf{k})]^2 + (J_k V)^2}} \right]. \quad (22)$$

Figure 2 plots the evolution of  $f$  and  $c$  electron spectra upon varying  $J_k/t$  at  $J_h/t = 1$ . As can be seen, the nearly flat hybridized bands for  $J_k/J_h \gg 1$  acquire appreciable dispersion upon reducing  $J_k/t$ . Consequently, the location of the QP gap  $\Delta_{qp}$  becomes  $J_k$  dependent drifting from  $\mathbf{k} = \pi$  in the large  $J_k/t = 4$  limit to  $\mathbf{k} = \pi/2$  at  $J_k/t = 1$ , see Figs. 2(a)-2(c) and Figs. 2(e)-2(g).

- Vanishing hybridization order parameter  $V = 0$  such that the  $f$  and  $c$  layers are fully decoupled.

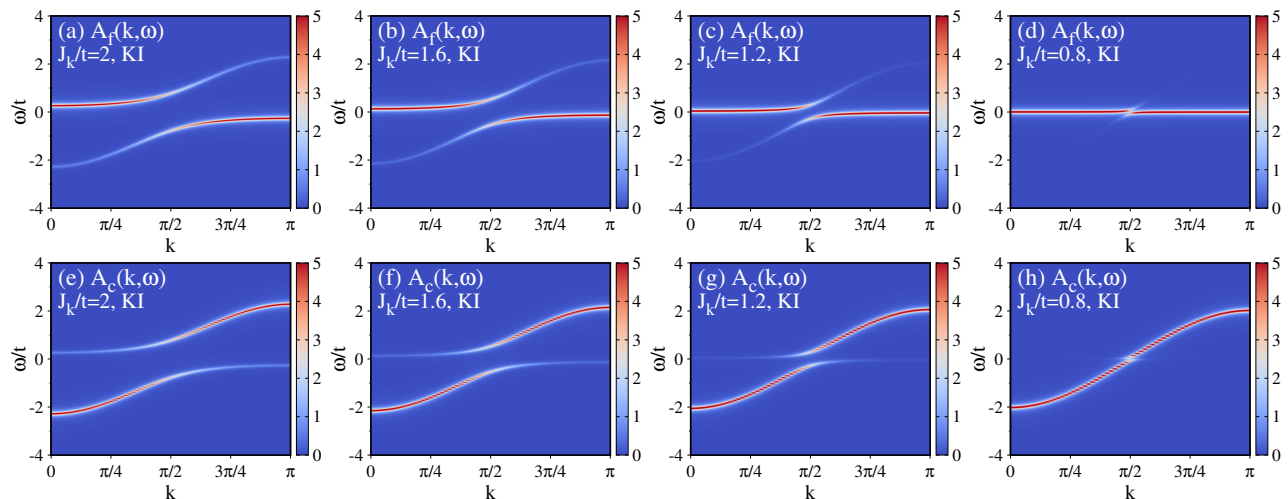


FIG. 1. (a)-(d)  $f$  fermion  $A_f(\mathbf{k}, \omega)$  and (e)-(h) conduction electron  $A_c(\mathbf{k}, \omega)$  spectral functions as obtained from the large- $N$  approach accounting for Kondo screening in the translationally invariant Kondo chain with  $J_h = 0$  for representative values of  $J_k/t$ .

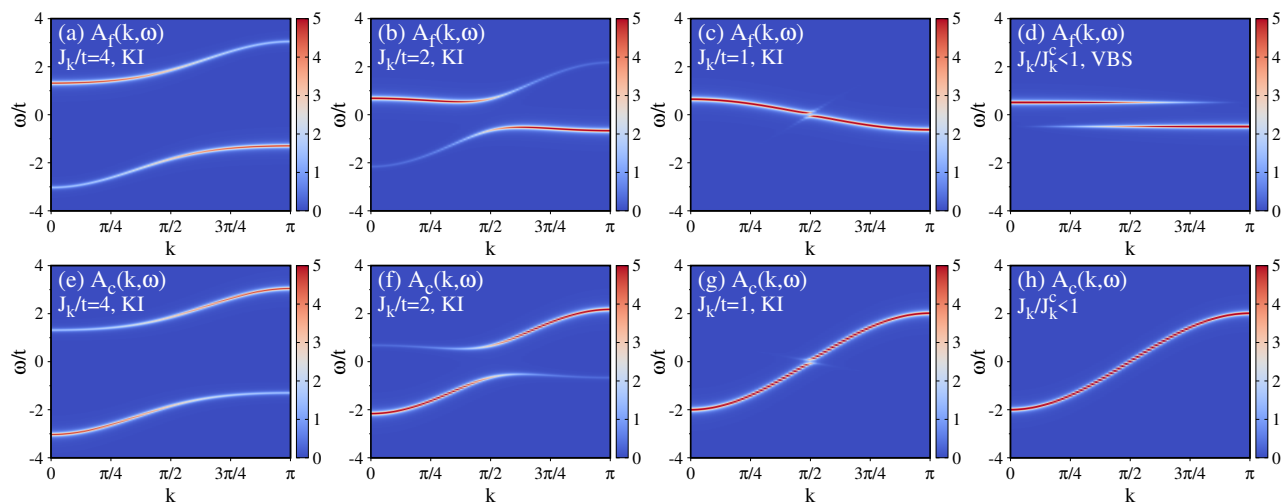


FIG. 2. (a)-(d)  $f$  fermion  $A_f(\mathbf{k}, \omega)$  and (e)-(h) conduction electron  $A_c(\mathbf{k}, \omega)$  spectral functions as obtained from the large- $N$  approach accounting for both Kondo screening and spinon description of the Kondo-Heisenberg chain with  $J_h/t = 1$  for representative values of  $J_k/t$ . Panels (a)-(c) and (e)-(g) correspond to self-consistent solutions with a uniform valence bond order parameter Ansatz, i.e.,  $\chi_{ij} = \chi_0$ . For  $J_k \leq J_k^c = 1.67t$  the ground state corresponds to the VBS phase where each  $f$  spin forms a dimer with only one of its two neighbors, i.e.,  $\chi_A = -1$  and  $\chi_B = 0$ , and no Kondo screening occurs,  $V = 0$ , see panels (d) and (h).

The self-consistency procedure for the  $f$  subsystem yields a saddle-point solution where each spin forms a dimer with only one of its two neighbors, i.e.,  $\chi_A \neq 0$  and  $\chi_B = 0$  [115, 116]. As a result,  $\chi_0 = \delta \equiv \chi$  and thus the dispersion relation of the  $f$  states

$$E_{\mathbf{k}}^{\pm} = \pm J_h \sqrt{\chi_0^2 \cos^2 k + \delta^2 \sin^2 k} \quad (23)$$

becomes completely localized with quasiparticle energies  $\pm J_h \chi$ , see Fig. 2(d). On the other hand, the conduction electron layer corresponds to a free electron gas whose energy spectrum is given by a

tight-binding dispersion relation without a gap, see Fig. 2(h). As we show it in Sec. III A 2 by explicitly performing self-consistent large- $N$  calculations using the full  $4 \times 4$  matrix in Eq. (17), the  $J_k = 0$  (or equivalently  $V = 0$ ) VBS ground state extends up to  $J_k^c/t = 1.67$ , i.e., at the mean-field level, VBS order is generically accompanied by vanishing Kondo screening [61–66].

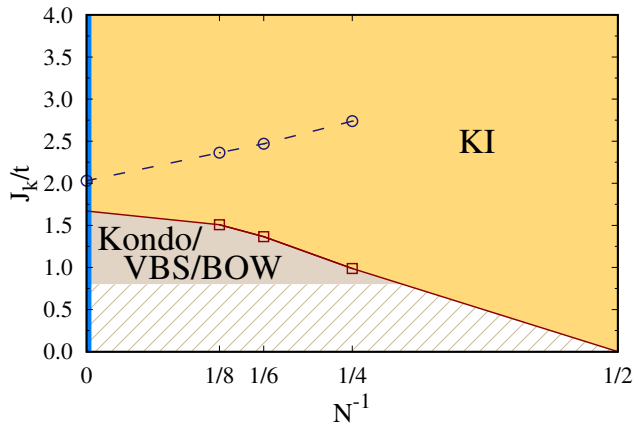


FIG. 3. The conjectured zero temperature phase diagram of the  $SU(N)$  Kondo-Heisenberg chain with  $J_h/t = 1$  hosts: (i) Kondo insulator (KI) state and (ii) valence bond solid (VBS) phase of  $f$  spins coexisting with both Kondo screening and a bond order wave (BOW) state of itinerant electrons. Available system sizes in QMC simulations determine the reachable energy scales of the model and restrict reliable studies to values of  $J_k/t \geq 0.8$  above the stripy region. The transition between the KI and VBS/BOW phases for  $N \geq 4$  (squares) is shown to belong to the 2D classical Ising universality class. The limit of infinite degeneracy  $\frac{1}{N} = 0$  represents a singular line (solid blue): The phase transition is of first order, the  $f$  and  $c$  layers become fully decoupled in the VBS phase, and the BOW state does not appear. Circles indicate the change in the position of the minimal quasiparticle (QP) gap in the KI state from  $\mathbf{k} = \pi/2$  at intermediate values of  $J_k/t$  to  $\mathbf{k} = \pi$  in the large  $J_k/t$  region reminiscent of the physics of the bare Kondo chain. For  $N = 2$ , the critical nature of the spin-1/2 Heisenberg antiferromagnetic chain [119] implies the instability towards the KI phase at any finite value of  $J_k/t$ . The  $N = 2$  data quality does not allow us to meaningfully estimate the QP gap at the  $\mathbf{k} = \pi$  point. Given a tiny  $\sim 10^{-4}$  QP residue at  $\mathbf{k} = \pi$ , we believe that the low energy physics will be dominated by QP excitations at the  $\mathbf{k} = \pi/2$  point.

### III. NUMERICAL RESULTS

#### A. $SU(N)$ Kondo-Heisenberg chain

In this section we explore the ground state as well as spin and single particle excitation spectra of the  $SU(N)$  Kondo-Heisenberg model. Throughout, we consider the value  $J_h/t = 1$ .

##### 1. Phase diagram

Figure 3 maps out the ground state phase diagram as a function of  $\frac{1}{N}$  and Kondo coupling  $J_k/t$  and provides a concise summary of our main findings. In the large Kondo coupling limit  $J_k/J_h \gg 1$ , the effect of the Heisenberg interaction can be neglected and the low energy physics should correspond to that of the bare Kondo chain with  $J_h = 0$ . We thus find a homogeneous KI phase

for each  $N$ .

Upon decreasing the Kondo coupling  $J_k/t$ , the Heisenberg interaction progressively dominates over the Kondo scale. As indicated by circles, it gives rise to a change in the position of the minimal quasiparticle gap in the KI state from  $\mathbf{k} = \pi$  consistent with a bare Kondo chain to the  $\mathbf{k} = \pi/2$  point. This effect is equally captured by the large- $N$  approach accounting for both Kondo screening and the spinon description of the Kondo-Heisenberg chain.

Given a dimerized ground state of the bare  $SU(N \geq 4)$  Heisenberg antiferromagnetic chain [76, 77], further reduction of  $J_k/t$  triggers a phase transition to the VBS phase of the  $f$  spins. While the finite size scaling of the QMC data is consistent with the 2D classical Ising universality class of the transition, the large- $N$  approach erroneously produces a direct first order phase transition.

Another difference between the QMC and large- $N$  methods concerns the nature of the ordered phase: The QMC data are consistent with VBS order coexisting with both Kondo screening and a BOW state displaying a dimerized kinetic energy of itinerant electrons. In contrast, at the mean-field level, the KI-VBS phase transition represents an example of the Kondo breakdown such that the  $f$  and  $c$  layers are fully decoupled, and thus the BOW phase does not appear.

Since both the relevant energy scales, i.e., dimer order and Kondo screening are generated fully dynamically in QMC simulations, reaching the genuine ground state becomes less tractable for small Kondo couplings and requires us to simulate exponentially long chains. Within the available system sizes  $L \leq 130$ , we are hence limited to values of  $J_k/t \geq 0.8$  above the stripy region in Fig. 3.

##### 2. Large- $N$ analysis

To account for the possible coexistence of dimer order and Kondo screening, we solve the saddle-point equations (18) for a unit cell with two sites  $A$  and  $B$  using the large- $N$  Hamiltonian matrix in Eq. (17). Figures 4(a)-4(c) show the ground state energy of the solutions we have found and the corresponding mean-field order parameters as a function of Kondo coupling  $J_k/t$ .

Despite initializing our large- $N$  calculations using different sets of the hybridization order  $V = \langle f_i^\dagger \hat{c}_i + h.c. \rangle$ , uniform  $\chi_0 = \frac{1}{2}(\chi_A + \chi_B)$ , and staggered  $\delta = \frac{1}{2}(\chi_A - \chi_B)$  valence bond order parameters, the self-consistent procedure yields only two distinct phases: (i) VBS state with fully decoupled dimers characterized by  $\delta = \chi_0 \neq 0$  and  $V = 0$  and (ii) homogeneous KI state with  $\delta = 0$ ,  $\chi_0 \neq 0$ , and  $V \neq 0$ . By comparing the ground state energies of these solutions, we find that the  $J_k = 0$  (or equivalently  $V = 0$ ) VBS phase persists as the ground state for a finite range of Kondo coupling  $J_k/t \leq 1.67$ . At this point, Kondo screening becomes competitive enough to compensate both the energy gain due to the formation of strong valence bond singlets in the VBS phase and a

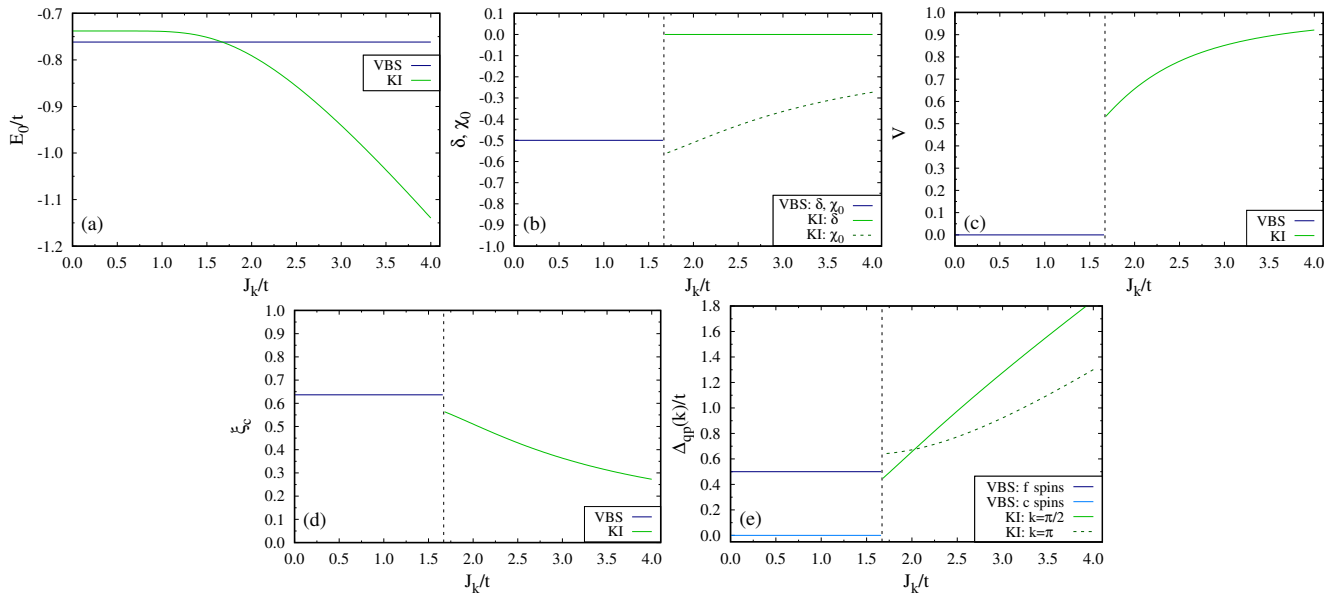


FIG. 4. Large- $N$  analysis of the Kondo-Heisenberg chain: (a) Ground state energy  $E_0/t$ , (b) valence bond  $\delta$ ,  $\chi_0$ , and (c) Kondo singlet  $V$  order parameters as a function of  $J_k/t$  reveal a direct first order phase transition at  $J_k^c/t = 1.67$  separating a VBS phase with fully decoupled  $f$  spin dimers ( $\delta = \chi_0 \neq 0$  and  $V = 0$ ) and a uniform KI state ( $\delta = 0$ ,  $\chi_0 \neq 0$ , and  $V \neq 0$ ). For completeness, we also show the evolution of (d) bond kinetic energy of the conduction electrons  $\xi_c$  and (e) quasiparticle gap  $\Delta_{qp}(\mathbf{k})$ . The latter is momentum independent in the VBS phase of the  $f$  layer and since  $V = 0$  it vanishes in the conduction electron layer. In the KI phase, the gap displays a crossover between the  $\mathbf{k} = \pi/2$  and  $\mathbf{k} = \pi$  points.

loss of the bond kinetic energy of conduction electrons  $\xi_c = \langle \hat{c}_i^\dagger \hat{c}_{i+1} + h.c. \rangle$  due to the formation of Kondo singlets with local moments, see Fig. 4(d). Consequently, a uniform KI phase becomes the ground state. As is apparent, the transition is signaled by a jump in each order parameter and thus is of first order. Given existing evidence for the first order nature of the VBS-KI transition in frustrated 2D lattices [61–66], it appears that frozen dimers in the realm of the large- $N$  approximation are generally accompanied by a vanishing of Kondo screening.

Finally, Fig. 4(e) illustrates the evolution of the quasiparticle gap. In the VBS phase, the dispersion relation of the  $f$  states is completely localized with momentum independent quasiparticle energies  $\pm J_h \chi_0$  such that  $\Delta_{qp}/t = 0.5$ . In contrast, the interplay between Kondo screening  $V$  and valence bond singlets  $\chi_0$  in the KI state determines the position of the minimal quasiparticle gap which shifts from  $\mathbf{k} = \pi/2$  for small  $J_k/t$  to the  $\mathbf{k} = \pi$  point in the large  $J_k/t$  region.

### 3. Critical behavior

In order to locate the phase boundary in Fig. 3 we carry out a finite size scaling analysis of the spin dimer

structure factor for the  $f$  spins:

$$\mathcal{D}_f(\mathbf{q}) = \frac{1}{L} \sum_{i,j} e^{i\mathbf{q}\cdot(\mathbf{i}-\mathbf{j})} \times \left( \langle \hat{\Delta}_{i,i+1} \hat{\Delta}_{j,j+1} \rangle - \langle \hat{\Delta}_{i,i+1} \rangle \langle \hat{\Delta}_{j,j+1} \rangle \right), \quad (24)$$

with  $\hat{\Delta}_{i,i+1} = \sum_{\mu,\nu} \hat{S}_{i,\nu}^{f,\mu} \hat{S}_{i+1,\mu}^{f,\nu}$ . Next, we calculate the renormalization group invariant correlation ratio

$$R_f = 1 - \frac{\mathcal{D}^f(\mathbf{Q} - \delta\mathbf{q})}{\mathcal{D}^f(\mathbf{Q})}, \quad (25)$$

where  $\mathbf{Q} = \pi$  is the ordering wavevector and  $\delta\mathbf{q} = 2\pi/L$  is the smallest finite wavevector for a given system size  $L$ . As can be seen in Fig. 5,  $R_f$  scales to unity (zero) for ordered (disordered) states and shows a crossing point as a function of system size at the critical Kondo coupling  $J_k^c$ . The latter can be obtained accurately by noting that a two-fold degeneracy of the dimerized ground state implies the same critical behavior as the 2D Ising model, i.e., the correlation length exponent  $\nu = 1$  and the order parameter exponent  $\beta = 1/8$ . Indeed, using the scaling assumption

$$R_f = \mathcal{F}[(J_k/J_k^c - 1)L^{1/\nu}], \quad (26)$$

we obtain for  $L \geq 66$  and in the vicinity of the critical point, a decent data collapse of  $R_f$  shown in Figs. 6(a) ( $N = 4$ ), 6(c) ( $N = 6$ ), and 6(e) ( $N = 8$ ). It allows us to estimate critical couplings  $J_k^c/t = 0.987(2)$  for  $N = 4$ ,



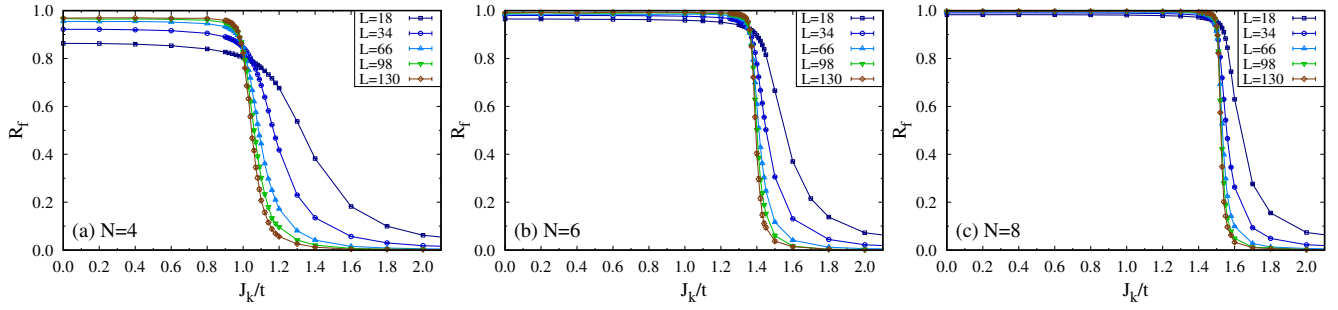


FIG. 5. Correlation ratio  $R_f$  from the structure factor of  $f$  spin dimer correlations in the  $SU(N)$  Kondo-Heisenberg chain: (a)  $N = 4$ ; (b)  $N = 6$ , and (c)  $N = 8$ .

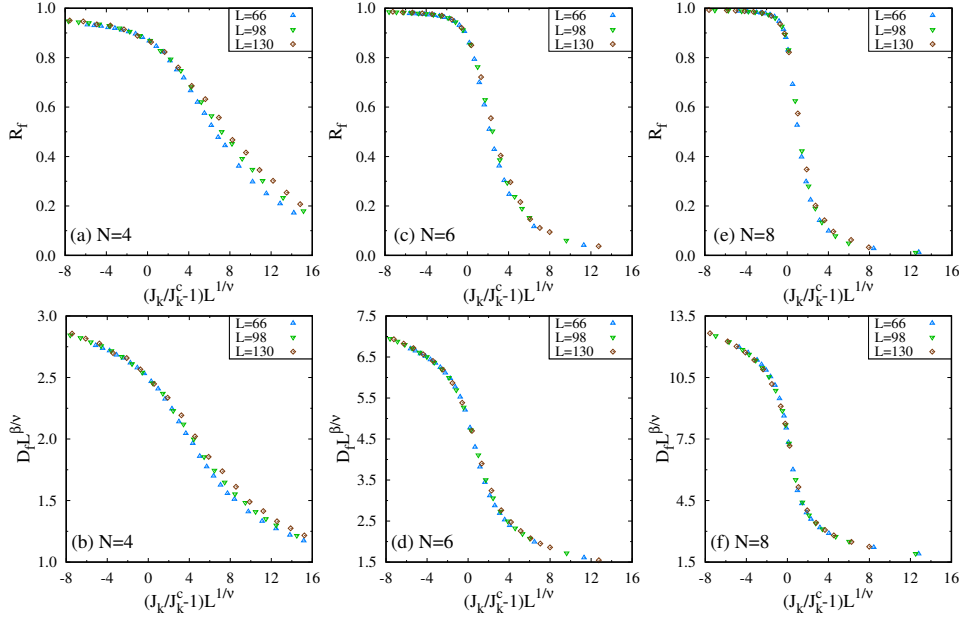


FIG. 6. Data collapse for the  $L \geq 66$   $SU(N)$  Kondo-Heisenberg chains using the 2D Ising critical exponents  $\nu = 1$  and  $\beta = 1/8$  of the: (a), (c), and (e) correlation ratio  $R_f$  from the structure factor of  $f$  spin dimer correlations and (b), (d), and (f) the dimer order parameter  $D_f = \sqrt{\frac{D_f(q=\pi)}{L}}$  for  $N = 4$  (left),  $N = 6$  (middle), and  $N = 8$  (right).

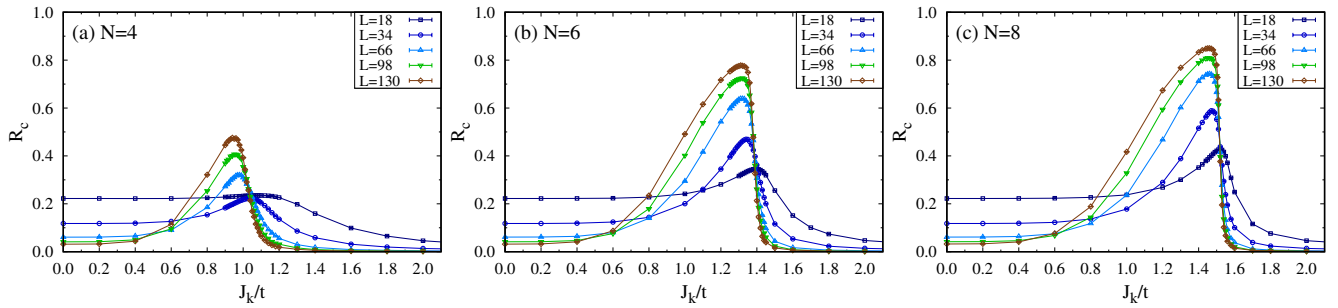


FIG. 7. Correlation ratio  $R_c$  from the structure factor of kinetic dimer correlations for the conduction electrons in the  $SU(N)$  Kondo-Heisenberg chain: (a)  $N = 4$ ; (b)  $N = 6$ , and (c)  $N = 8$ .

$J_k^c/t = 1.366(1)$  for  $N = 6$ , and  $J_k^c/t = 1.508(1)$  for  $N = 8$ . Clearly, an enhanced  $SU(N)$  symmetry favors the dimerized ground state and shifts the critical coupling to larger values of  $J_k$  in accordance with the large- $N$

calculation predicting  $J_k^c/t = 1.67$ .

To further assess the consistency of our numerical data with the 2D Ising universality class, we consider a dimer

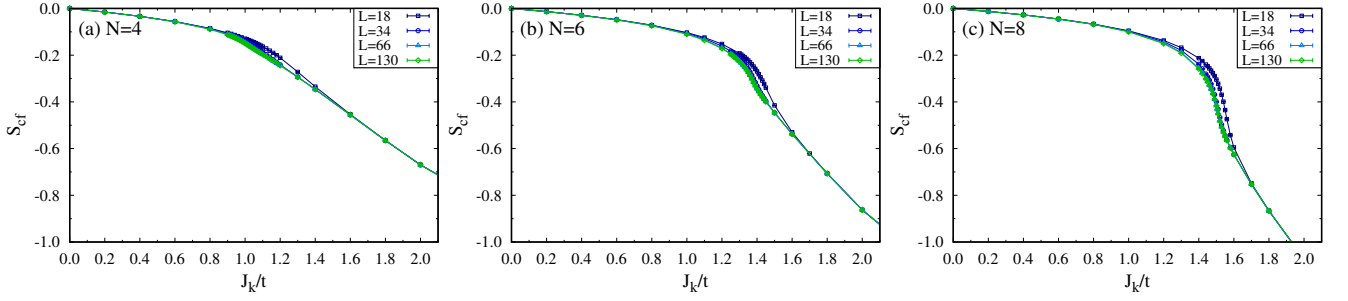


FIG. 8. Local spin-spin correlation function  $S_{cf}$  as a function of  $J_k/t$  in the  $SU(N)$  Kondo-Heisenberg chain with a different length  $L$ : (a)  $N = 4$ ; (b)  $N = 6$ , and (c)  $N = 8$ .

order parameter  $D_f = \sqrt{\frac{\mathcal{D}_f(\mathbf{q}=\pi)}{L}}$  which shall satisfy the finite size scaling relation

$$D_f L^{\beta/\nu} = \mathcal{F}[(J_k/J_k^c - 1)L^{1/\nu}], \quad (27)$$

involving both the critical exponents  $\nu$  and  $\beta$ . The corresponding scaling collapses are shown in Figs. 6(b) ( $N = 4$ ), 6(d) ( $N = 6$ ), and 6(f) ( $N = 8$ ) and lead to critical Kondo couplings consistent within error bars with the previous estimates.

Interestingly, even though it is not the  $SU(N)$  spin symmetry that gets broken at the phase transition, changing  $N$  modifies the shape of the scaling function  $\mathcal{F}$  such that it progressively develops a step-like behavior. Since a correlation ratio  $R$  generically scales as  $(\xi/L)^2$  where  $\xi$  is the correlation length [120], a constant value of  $R$  for  $J_k > J_k^c$  implies no divergence of the correlation length and thus a first order phase transition. This line of arguing is consistent with the large- $N$  analysis predicting the first order nature of transition in the limit of infinite degeneracy  $N \rightarrow \infty$ . We believe, however, that it is a singular point and quantum critical fluctuations restore the 2D classical Ising universality class close to  $J_k^c$  at any finite  $N$  even though the critical region itself shrinks. We also note that the development of a step-like scaling function helps to reduce the finite size effect and allows one to obtain a nice data collapse over a broader interval around  $J_k^c$ .

It is very natural to expect that the translationally invariant conduction electrons gas coupled via a Kondo coupling  $J_k > 0$  to a dimerized lattice of magnetic impurities will spontaneously reduce its symmetry by acquiring the same dimerization pattern as the local  $f$  spins. To confirm this expectation and quantify the degree of dimerization in the conduction electron layer, we measure the kinetic energy dimer structure factor

$$\mathcal{K}_c(\mathbf{q}) = \frac{1}{L} \sum_{i,j} e^{i\mathbf{q}\cdot(i-j)} \times \left( \langle \hat{K}_{i,i+1} \hat{K}_{j,j+1} \rangle - \langle \hat{K}_{i,i+1} \rangle \langle \hat{K}_{j,j+1} \rangle \right), \quad (28)$$

with  $\hat{K}_{i,i+1} = \hat{c}_i^\dagger \hat{c}_{i+1} + h.c.$  Figure 7 plots the corre-

sponding correlation ratio

$$R_c = 1 - \frac{\mathcal{K}^c(\mathbf{Q} - \delta\mathbf{q})}{\mathcal{K}^c(\mathbf{Q})}, \quad (29)$$

for  $\mathbf{Q} = \pi$  as a function of  $J_k/t$ . On the one hand, the observed increase of  $R_c$  around  $J_k^c$  is indicative of strong BOW fluctuations. Given the growth of  $R_c$  with a system size  $L$ , we expect the onset of long range BOW order in the thermodynamic limit. On the other hand, by considering a finite spin gap  $\Delta_s$  in the dimerized ground state of the bare  $SU(N \geq 4)$  Heisenberg chain, one could argue in favor of a simple picture of a complete decoupling of both layers in the limit  $J_k/\Delta_s \ll 1$ .

To address this issue, we plot in Fig. 8 the local spin-spin correlator

$$S_{cf} = \frac{N}{(N^2 - 1)L} \sum_i \sum_{a=1}^{N^2-1} \langle \hat{c}_i^\dagger T^a \hat{c}_i \cdot \hat{f}_i^\dagger T^a \hat{f}_i \rangle. \quad (30)$$

Here  $T^a$  corresponds to the generators of  $SU(N)$  with the normalization condition:  $\text{Tr} T^a T^b = \frac{\delta_{a,b}}{2}$ . As is apparent, this quantity remains finite at any  $J_k > 0$  such that the picture of a complete decoupling never holds. Thus we believe that simulations performed on sufficiently long chains would reveal the signature of coexisting VBS and BOW orders as soon as  $J_k > 0$ , see also Ref. [75]. Indeed, given that the long distance behavior of correlation functions determines the low energy physics, it is obvious that limited system sizes used in our QMC simulations act as the energy cutoff for long-wavelength dimer fluctuations. On the one hand, already our shortest  $L = 18$  chain is sufficient to produce the increase of  $R_c$  around the quantum critical point  $J_k^c$  where quantum fluctuations diverge and become scale invariant. On the other hand, on moving away from  $J_k^c$  in the VBS phase while keeping the system size fixed, one inevitably arrives at the regime with effectively frozen  $f$  spin dimers. This regime is captured by the large- $N$  theory and, as we have explicitly shown, fails to account for the BOW phase arising from VBS order and erroneously leads to the breakdown of Kondo screening. This implies that to provide a definite answer concerning the fate of Kondo screening it is imperative to control first the energy scale of the BOW state.

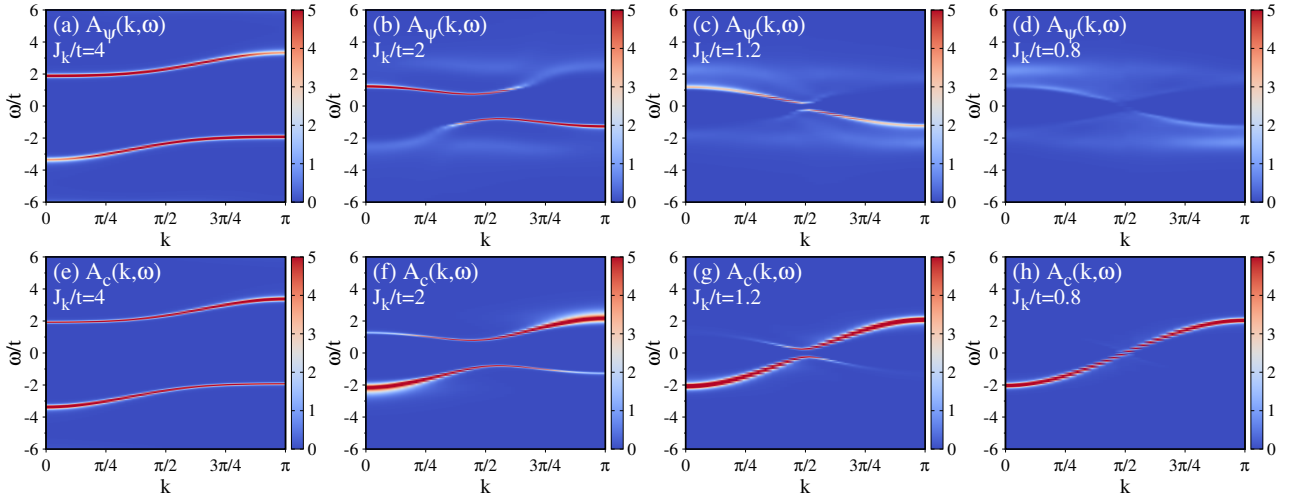


FIG. 9. (a)-(d) Composite fermion  $A_\psi(\mathbf{k}, \omega)$  and (e)-(h) conduction electron  $A_c(\mathbf{k}, \omega)$  spectral functions of the  $L = 66$  SU(4) Kondo-Heisenberg chain for representative values of  $J_k/t$ ; the critical Kondo coupling  $J_k^c/t = 0.987(2)$ .

In fact, Fig. 7 allows one to estimate the minimal value of  $J_k/t$  above which system sizes  $L$  available in our QMC simulations guarantee that the conduction electrons are subject to fluctuating  $f$  spin dimers. Indeed, as a function of  $L$ , it is possible to overcome the initial decrease of  $R_c$  for  $J_k/t \geq 0.8$ . In contrast, for smaller values of  $J_k/t$  and up to our largest system sizes  $L = 130$ , we are not able anymore to generate an increase of  $R_c$  indicating that our results are biased by finite size effects.

Finally, it is noteworthy to point out a progressively steeper evolution of the local spin-spin correlation  $S_{cf}$  across the transition point, see Figs. 8(a)-8(c). A similar tendency is also observed in Fig. 6 where the enlarged SU( $N$ ) symmetry of the model drives the onset of a step-like behavior of the scaling function  $\mathcal{F}$ . The similarity in the response to the enlarged SU( $N$ ) symmetry seen in  $\mathcal{F}$  and  $S_{cf}$  follows from the fact that the latter is directly proportional to the free energy derivative  $\frac{\partial F}{\partial J_k}$ . Hence, a discontinuity in  $S_{cf}$  upon varying  $J_k/t$  would signal a first order transition. The latter is expected on the basis of large- $N$  calculations to take place only in the limit of infinite degeneracy  $N \rightarrow \infty$ .

#### 4. Single particle spectra

With restrictions on a minimal value of  $J_k/t \simeq 0.8$  imposed by the available system sizes in QMC simulations in mind, we proceed to elucidate the fate of Kondo screening across the phase diagram in Fig. 3.

To this end, we calculate the evolution of the momentum resolved spectral function of the composite fermion  $A_\psi(\mathbf{k}, \omega) = -\frac{1}{\pi} \text{Im} G_\psi^{\text{ret}}(\mathbf{k}, \omega)$  with  $G_\psi^{\text{ret}}(\mathbf{k}, \omega) = -i \int_0^\infty dt e^{i\omega t} \sum_\sigma \langle \{ \hat{\psi}_{\mathbf{k}, \sigma}(t), \hat{\psi}_{\mathbf{k}, \sigma}^\dagger(0) \} \rangle$ . In the Kondo screened phase  $A_\psi(\mathbf{k}, \omega)$  displays well defined quasiparticle poles whose dispersion relation follows that of the

$f$  fermion in the large- $N$  approach [36]. In contrast, a continuum of excitations in  $A_\psi(\mathbf{k}, \omega)$  signals the decay of a composite quasiparticle and points out the breakdown of a coherent lattice Kondo effect [10]. To identify the origin of dominant spectral features, we have equally calculated the electronic excitation spectrum for the conduction electrons  $A_c(\mathbf{k}, \omega) = -\frac{1}{\pi} \text{Im} G_c^{\text{ret}}(\mathbf{k}, \omega)$ .

To begin with let us consider the SU(4) model. Figures 9(a)-9(c) [9(e)-9(g)] illustrate the evolution of  $A_\psi(\mathbf{k}, \omega)$  [ $A_c(\mathbf{k}, \omega)$ ], respectively, upon going through the uniform Kondo screened phase. As a function of decreasing  $J_k/t$ , there is a continuous change of the wavevector which determines the low energy dynamics from  $\mathbf{k} = \pi$  to  $\mathbf{k} = \pi/2$ . Thus, the QMC data validate the findings within the large- $N$  approach accounting for both Kondo screening and the spinon description of the Kondo-Heisenberg chain, see Fig. 2(a)-2(c).

This result is surprising and deserves more attention. The surprise comes from early QMC studies of a single-hole dynamics in the half-filled 2D Kondo-Hubbard model with an extra Hubbard interaction  $U$  in the conduction band [21]. Given that the low energy hole dynamics between the Kondo and Hubbard models is controlled by different wavevectors, it is not obvious how these conflicting tendencies can be accommodated in a single effective electronic dispersion when both interactions are brought together. It turns out, however, that irrespective of values of  $U/t$ , the lowest energy hole states occur for  $J_k/t > 0$  at  $\mathbf{k} = (\pi, \pi)$  as in the pure Kondo lattice model. The supremacy of Kondo and RKKY interactions in determining the low energy band structure of the uniform KI state can be nevertheless broken down by the Heisenberg interaction between the local moments by shifting the position of the minimal gap from  $\mathbf{k} = \pi$  at large Kondo coupling  $J_k/t = 4$ , see Fig. 9(a), to  $\mathbf{k} = \pi/2$  at  $J_k/t = 1.2$  in Fig. 9(c). Importantly, this change does not require any extra spontaneous symmetry breaking.

Hence, a rigid shift of the hybridized bands upon doping would lead to a Lifshitz transition where the Fermi surface topology in the heavy fermion liquid changes from two to four points. This guarantees that the Luttinger volume remains preserved [51].

This piece of information has consequences for the interpretation of experimental data. It implies that the form of the low energy band structure allows one to identify, at least in a 1D setup, the origin of the dominant magnetic interaction between the local  $f$  spins: A direct Heisenberg exchange vs. the indirect RKKY interaction. It remains to be verified numerically if and how our result carries over to higher dimensions.

We proceed now to discuss electronic spectra at our smallest value of  $J_k/t \simeq 0.8$  in the ordered phase. As shown in Fig 9(d), a faint composite fermion band extending to the  $\mathbf{k} = \pi$  point persists in the presence of fluctuating  $f$  spin dimers. The latter are compatible with Kondo screening and trigger BOW fluctuations in the conduction electron layer. Both effects modify its tight binding cosine band which acquires a small gap at the Fermi level and develops backfolded shadow bands tracking the composite fermion band, see Fig 9(h). As we show latter on, the gap opens up exponentially and thus it requires correspondingly large system sizes to simulate which renders the BOW phase intractable in the weak coupling limit  $J_k/t < 0.8$ .

The above findings contrast with a large- $N$  outcome in Fig. 2(d). It displays a fully localized, i.e., flat,  $f$  electron spectrum specific to VBS order with frozen isolated dimers accompanied by the breakdown of Kondo screening. As a consequence, the conduction electrons are fully decoupled from the localized spins and their dispersion relation recovers a tight binding cosine form, see Fig. 2(h).

Unfortunately, a small critical coupling  $J_k^c/t \simeq 1$  of the SU(4) model leads to a low quasiparticle intensity and hampers a detailed analysis of spectral properties in the ordered phase. Given that an enhanced SU( $N$ ) symmetry favors the dimerized ground state by shifting the critical coupling to larger values of  $J_k/t$ , one way around this problem is to consider a system with larger  $N$ .

Thus we consider the SU(8) model for which  $J_k^c/t \simeq 1.5$ . Here, our primary focus is on tracking the evolution of spectra in the vicinity of  $J_k^c$ , see Fig. 10. Given a relatively high symmetry of the SU(8) model bringing the underlying physics closer to the large- $N$  limit, our evidence of the 2D Ising universality found in Sec. III A 3 does not necessarily guarantee persistent Kondo screening in the ordered phase. Indeed, VBS/BOW order alone is sufficient to gap out both the charge and spin degrees of freedom such that the same universality would also hold in the case of the full collapse of Kondo screening at the critical Kondo coupling. Nevertheless, the observed continuous evolution of composite fermion quasiparticle at  $\mathbf{k} = \pi$  confirms that quantum critical dimer fluctuations do not destroy Kondo screening. Moreover, the onset of

long range VBS/BOW order enriches both the  $A_\psi(\mathbf{k}, \omega)$  and  $A_c(\mathbf{k}, \omega)$  spectral functions with extra features such that one can distinguish around  $\mathbf{k} = \pi/2$  a total of four bands, see, e.g., Figs. 10(b) and 10(g).

To get some further insight into the physical origin of these bands, it is worthwhile to draw a comparison between the QMC data and large- $N$  modeling of spectral functions as accounted for by the Hamiltonian in Eq. (17). To this end, we focus on the critical value  $J_k^c/t = 1.67$  and consider the hybridization  $V$  and dimerization  $\delta$  amplitudes as tuning parameters while keeping fixed  $\chi_0 = -0.5$ . We first impose a moderate dimerization  $\delta = 0.5\chi_0$  and weaken the Kondo screening amplitude from  $V/t = -0.528$ , through  $V/2$ , down to  $V/3$ , see Figs. 11(a)-11(c) with  $A_\psi(\mathbf{k}, \omega)$  and 11(e)-11(g) with  $A_c(\mathbf{k}, \omega)$ . As can be seen, the combined effect of Kondo screening and broken translation symmetry gives rise to a four band electronic structure around  $\mathbf{k} = \pi/2$ . The two inner weakly dispersive bands have nearly pure  $f$  character while the two outer bands stem predominantly from the cosine band of  $c$  electrons which acquired both a gap and a pronounced backfolding. The latter reflects a doubling of the unit cell due to a dimerized kinetic energy of the conduction electrons emergent in response to the VBS pattern of  $f$  spins.

Upon decreasing  $V/t$ , the inner bands in  $A_f(\mathbf{k}, \omega)$  bend towards each other while their backfolded segments lose the spectral weight around  $\mathbf{k} = \pi/2$ . Due to the total spectral sum rule, the weight reappears in the corresponding part of  $A_c(\mathbf{k}, \omega)$  forming the "missing" segments of the cosine band. Meanwhile, the lowest energy part of the outer bands in  $A_f(\mathbf{k}, \omega)$  flattens and gains the intensity. Both effects are further enhanced by a stronger dimerization  $\delta = 0.8\chi_0$ , see Fig. 11(d). Hence, a starting point to understand the resultant spectrum  $A_f(\mathbf{k}, \omega)$  is a fully dimerized system with two flat bands shown in Fig. 2(d). A weak hybridization with the conduction electron band via the Kondo effect breaks each of the dimerized bands into outer and inner segments. The latter carries less spectral weight close to the  $\mathbf{k} = \pi/2$  point and its backfolded part displays a strong modulation of spectral intensity so as to fulfill the total spectral sum rule. Likewise, in the limit of strong dimerization, the cosine band in the conduction electron spectrum  $A_c(\mathbf{k}, \omega)$  is broken into four pronounced segments and is accompanied by backfolded shadow bands, see 11(h).

By comparing Fig. 10(d) with Fig. 11(d) and Fig. 10(h) with Fig. 11(h), it becomes clear that the large- $N$  approach gives good overall account of the four band structure seen in both  $A_\psi(\mathbf{k}, \omega)$  and  $A_c(\mathbf{k}, \omega)$ . Hence we trace the occurrence of these four bands back to the coexistence of Kondo screening and VBS/BOW order. Given that creating a Kondo singlet in the VBS phase requires the breakup of a  $f$  spin dimer, it is tempting to interpret this coexistence as a partial Kondo screening along the imaginary time axis — at a given time  $\tau$ , a finite fraction of the local moments is paired into intersite dimer singlets while the rest form Kondo singlets with conduc-

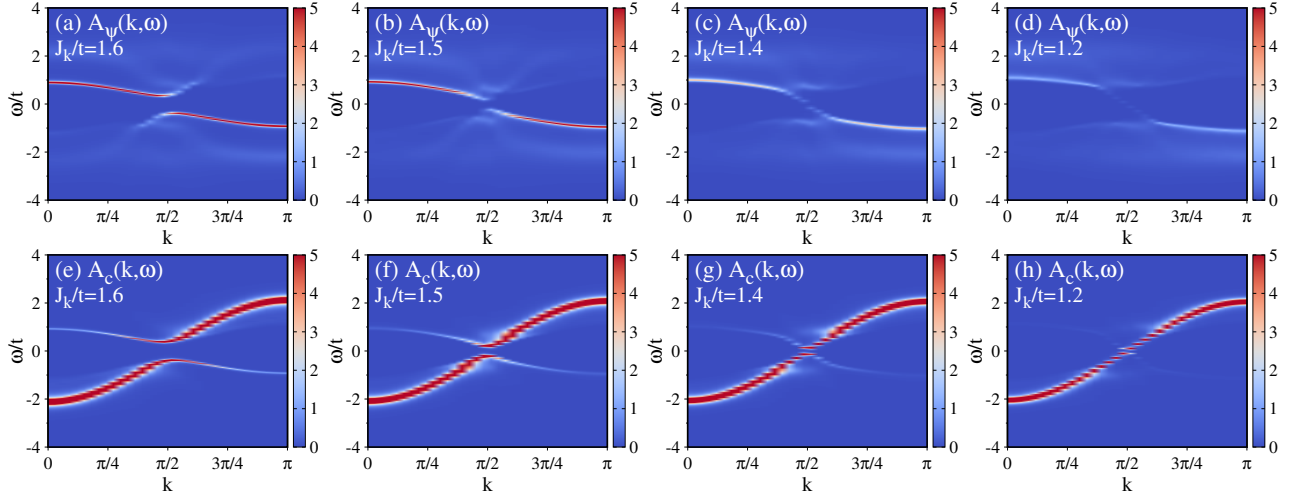


FIG. 10. Evolution of (a)-(d) composite fermion  $A_\psi(\mathbf{k}, \omega)$  and (e)-(h) conduction electron  $A_c(\mathbf{k}, \omega)$  spectral functions of the  $L = 66$  SU(8) Kondo-Heisenberg chain across the critical coupling  $J_k^c/t = 1.508(1)$ .

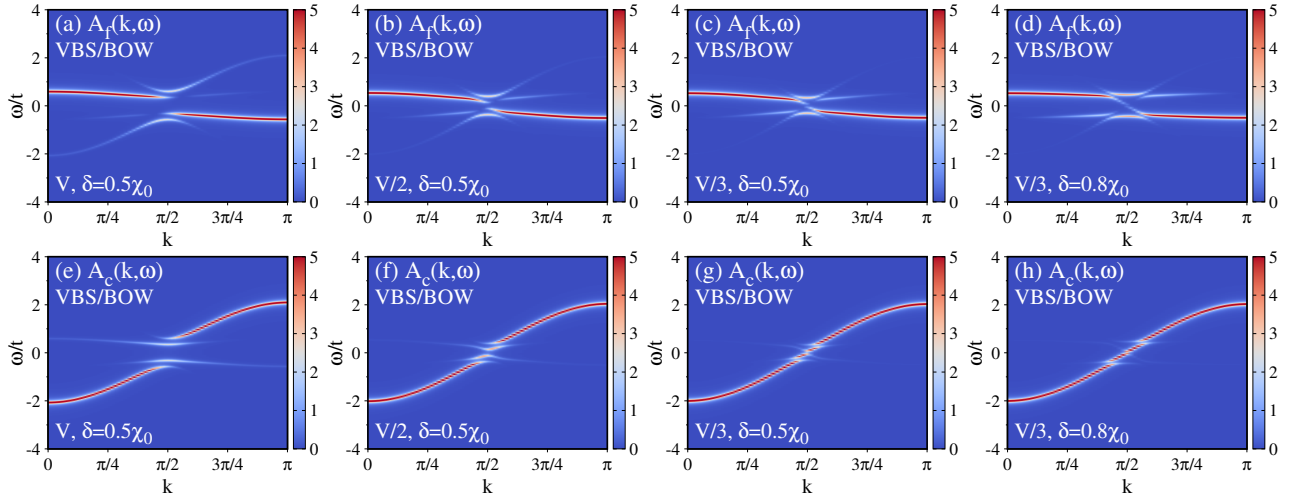


FIG. 11. (a)-(d)  $f$  fermion  $A_f(\mathbf{k}, \omega)$  and (e)-(h) conduction electron  $A_c(\mathbf{k}, \omega)$  spectral functions as obtained from the large- $N$  approach accounting for both Kondo screening and spinon description of the Kondo-Heisenberg chain at  $J_k^c/t = 1.67$  and  $J_h/t = 1$ . We assume here a two-site unit cell with an alternating between bonds  $A$  and  $B$  valence bond order parameter, i.e.,  $\chi_{A,B} = \chi_0 \pm \delta$ , and consider hybridization  $V$  and dimerization  $\delta$  amplitudes as tuning parameters. In all panels  $V/t = 0.528$  and  $\chi_0 = -0.5$ .

tion electron spins. Below we test this interpretation by looking at the evolution of spin excitation spectra.

### 5. Spin excitation spectra

In the Lehmann representation, the dynamical spin structure factor  $S(\mathbf{q}, \omega)$  reads

$$S(\mathbf{q}, \omega) \equiv \pi \sum_n |\langle \Psi_n | \hat{S}_{\mathbf{q}} | \Psi_0 \rangle|^2 \delta(E_n - E_0 - \omega) \quad (31)$$

where  $\hat{S}_{\mathbf{q}} = \frac{1}{\sqrt{L}} \sum_i e^{i\mathbf{q}\cdot\mathbf{i}} \hat{S}_i$  and  $\hat{H}|\Psi_n\rangle = E_n|\Psi_n\rangle$ . The SU( $N$ ) version of the imaginary time spin-spin correlator,

$$S(\mathbf{q}, \tau) = \frac{1}{N^2 - 1} \sum_{\mu, \nu} \langle \Psi_0 | \hat{S}_{\mathbf{q}, \mu}^\mu(\tau) \hat{S}_{-\mathbf{q}, \mu}^\nu | \Psi_0 \rangle, \quad (32)$$

where  $\hat{S}_{\mathbf{q}, \nu}^\mu$  are Fourier transformed SU( $N$ ) generators defined in Eq. (5), is directly measured in QMC simulations and related to the real frequency observable by

$$S(\mathbf{q}, \tau) = \frac{1}{\pi} \int d\omega e^{-\tau\omega} S(\mathbf{q}, \omega). \quad (33)$$

For the analytical continuation of the QMC data, we have used the ALF-2.0 implementation [112] of the stochastic maximum entropy method [113, 114]. In addition

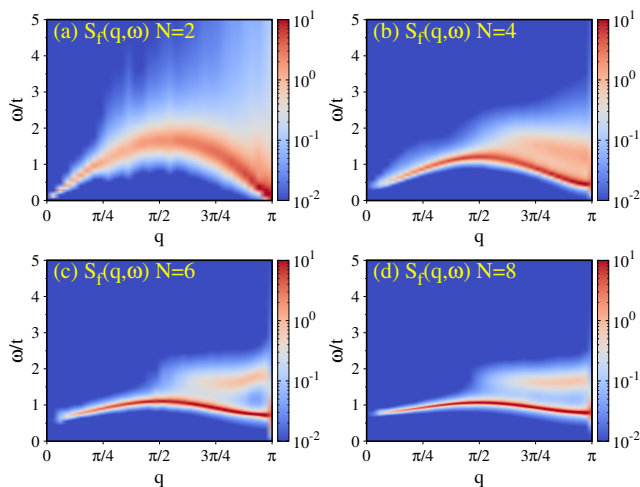


FIG. 12. Dynamical spin structure factor  $S_f(\mathbf{q}, \omega)$  of the bare  $L = 66$   $SU(N)$  Heisenberg chain: (a)  $N = 2$ ; (b)  $N = 4$ ; (c)  $N = 6$ , and (d)  $N = 8$ .

to  $S(\mathbf{q}, \omega)$  corresponding to the total spin, we have separately calculated the  $f$  spin  $S_f(\mathbf{q}, \omega)$  and conduction electron spin  $S_c(\mathbf{q}, \omega)$  excitation spectra. Having both quantities at hand helps to clarify the origin of distinct features in  $S(\mathbf{q}, \omega)$ .

The salient difference between the bare Heisenberg and Kondo chains concerns the nature of elementary spin excitations. In the spin-1/2 Heisenberg antiferromagnetic chain, the key elementary excitations are gapless spinons [121–123]. As shown in Fig. 12, a spontaneous dimerization present in the  $SU(N \geq 4)$  version of the Heisenberg chain gaps out the spin degrees of freedom but it clearly leaves spinons as the fundamental excitations above the spin gap, see also Ref. [72].

In contrast, the primary excitations of a bare Kondo chain correspond to gapped triplons [43]. The latter have a composite character involving both the  $f$  moments and conduction electron spins. Thus, the relative importance of Heisenberg versus Kondo interactions should be reflected in the evolution of spin excitation spectrum upon tuning the value of  $J_k/t$ .

At large  $J_k/t = 4$ , see Fig. 13(a), the dynamical (total) spin structure factor  $S(\mathbf{q}, \omega)$  is consistent with that of a pure Kondo chain and exhibits a low energy triplon mode corresponding to bound electron-hole pairs. The bound triplon shows a minimal gap at the  $\mathbf{q} = \pi$  wavevector and becomes washed out upon merging in the particle-hole continuum whose energy threshold [dashed line in Figs. 13(a)–13(d)] is given by the two particle charge gap  $2\Delta_{qp}$ . Figures 13(e) and 13(i) plot the corresponding  $f$  spin  $S_f(\mathbf{q}, \omega)$  and conduction electron spin  $S_c(\mathbf{q}, \omega)$  excitation spectra. As expected for the Kondo screened phase [124–126], both quantities display the same support but carry different spectral weights.

Reducing  $J_k/t$  modifies the spectrum so as to reflect the emerging Heisenberg spin physics. It brings about (i) softening of the triplon mode in the long-wavelength

limit  $\mathbf{q} = 0$  such that it gradually acquires a concave dispersion and (ii) a buildup of incoherent spectral weight around  $\mathbf{q} = \pi$ , just above the triplon mode, see Fig. 13(c). The latter is also seen in the  $f$  spin spectrum  $S_f(\mathbf{q}, \omega)$  in Fig. 13(g). The enhanced spectral intensity concentrated close to the lower boundary of the spectrum is a good indicator of fractional spinon excitations [117, 127, 128]. Thus it is tempting to identify it as the two-spinon continuum. As shown in Fig. 13(k), the lowest edge of the conduction electron spin spectrum  $S_c(\mathbf{q}, \omega)$  continues to display, albeit with strongly reduced weight around  $\mathbf{q} = \pi/2$ , the same support as the  $f$  spin spectrum  $S_f(\mathbf{q}, \omega)$ . On the other hand, a large majority of spectral weight in  $S_c(\mathbf{q}, \omega)$  above the charge gap is located on the upper boundary of the spectrum as expected for the particle-hole continuum of a nearly free conduction electron gas.

Figure 13(d) plots  $S(\mathbf{q}, \omega)$  at  $J_k/t = 0.8$  in the ordered phase. In the long-wavelength limit  $\mathbf{q} = 0$ ,  $S(\mathbf{q}, \omega)$  develops a nearly gapless linear mode. The latter is also resolved in the conduction electron spin spectrum  $S_c(\mathbf{q}, \omega)$ , see Fig. 13(l), being a consequence of the exponentially small single particle gap. The softening of conduction electron spin excitations is also seen at  $\mathbf{q} = \pi$ . Nevertheless, a fingerprint of electron-hole binding is still noticeable in  $S_c(\mathbf{q}, \omega)$  as a faint low energy image of the  $f$  spin excitations emerging below the particle-hole continuum sufficiently away from  $\mathbf{q} = \pi$ , see the arrow in Fig. 13(l). These common spectral aspects shared by  $S_f(\mathbf{q}, \omega)$  and  $S_c(\mathbf{q}, \omega)$  signify a remnant Kondo screening [124–126]. Meanwhile, a striking resemblance of the  $f$  spin spectrum  $S_f(\mathbf{q}, \omega)$ , see Fig. 13(h), to that of the corresponding isolated Heisenberg chain in Fig. 12(b) is very suggestive of the two-spinon excitations.

The coexistence of distinct spectral features brought about by Kondo and Heisenberg interactions across the phase transition is more tractable in the spin dynamics of the  $SU(8)$  case shown in Fig. 14. In addition to the two-spinon continuum, other prominent features include a nearly gapless linear mode at  $\mathbf{q} = 0$  occurring together with a remnant triplon excitation at slightly higher frequency, see Figs. 14(c) and 14(d). A faint image of the latter is also resolved in  $S_c(\mathbf{q}, \omega)$  both in the  $\mathbf{q} \rightarrow 0$  and  $\mathbf{q} \rightarrow \pi$  limits, see Figs. 14(k) and 14(l).

## 6. Spin and charge energy scales

Let us summarize this section with a compilation of the  $J_k/t$  dependence of the relevant energy scales in Fig. 15. All the quantities have been extrapolated to the thermodynamic limit based on QMC results on chains up to  $L = 130$  sites.

We begin with the single particle gap at  $\mathbf{k} = \pi/2$  shown in Figs. 15(a)–15(c). This quantity can be extracted by fitting the tail of the imaginary time Green’s function to the exponential form  $G(\mathbf{k}, \tau) \xrightarrow{\tau \rightarrow \infty} Z_{\mathbf{k}} e^{-\Delta_{qp}(\mathbf{k})\tau}$ , where  $Z_{\mathbf{k}}$  is the quasiparticle residue of the doped hole

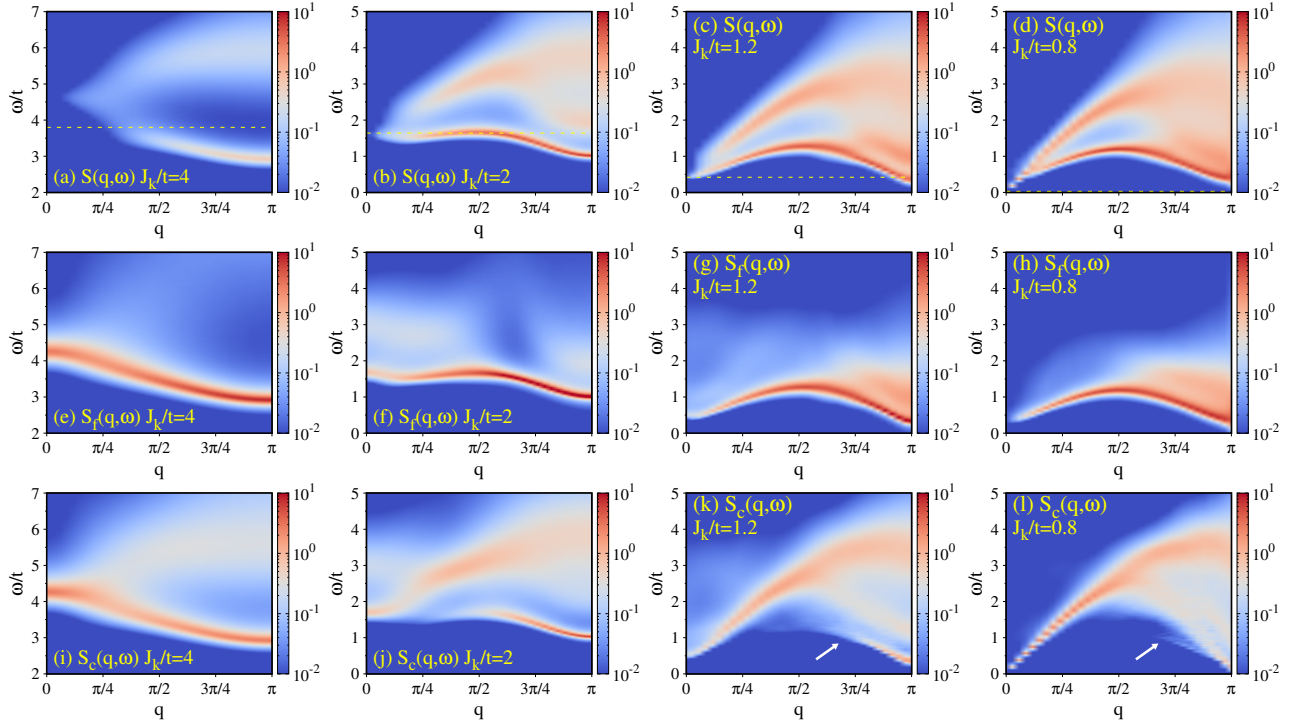


FIG. 13. Dynamical spin structure factor of the  $L = 66$   $SU(4)$  Kondo-Heisenberg chain for: (a)-(d) total spin  $S(\mathbf{q}, \omega)$ ; (e)-(h)  $f$  spin  $S_f(\mathbf{q}, \omega)$ , and (i)-(l) conduction electron spin  $S_c(\mathbf{q}, \omega)$  for values of  $J_k/t$  as in Fig. 9. Dashed lines indicate the particle-hole continuum threshold; the arrows help to track the image of a remnant triplon mode.

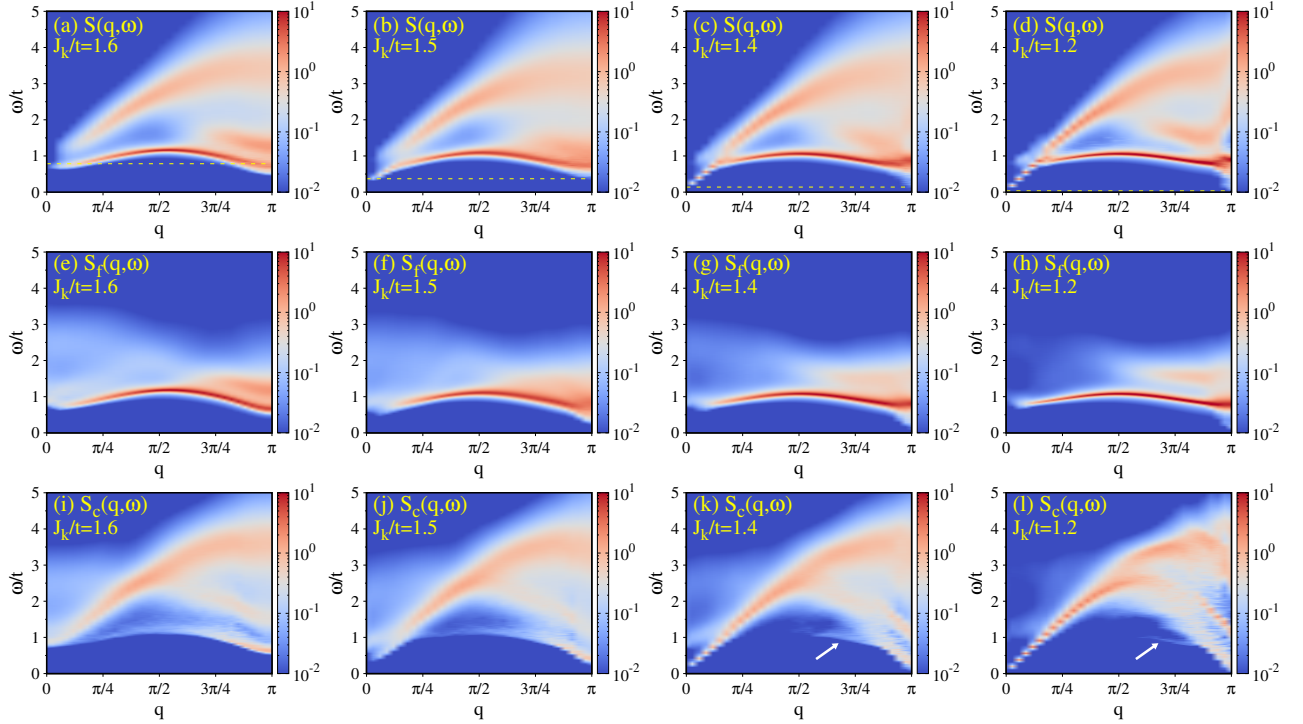


FIG. 14. Dynamical spin structure factor of the  $L = 66$   $SU(8)$  Kondo-Heisenberg chain for: (a)-(d) total spin  $S(\mathbf{q}, \omega)$ ; (e)-(h)  $f$  spin  $S_f(\mathbf{q}, \omega)$ , and (i)-(l) conduction electron spin  $S_c(\mathbf{q}, \omega)$  for values of  $J_k/t$  as in Fig. 10. Dashed lines indicate the particle-hole continuum threshold; the arrows help to track the image of a remnant triplon mode.

at momentum  $\mathbf{k}$  and frequency  $\omega = -\Delta_{qp}$ . To assess the quality of the data we consider both the compos-

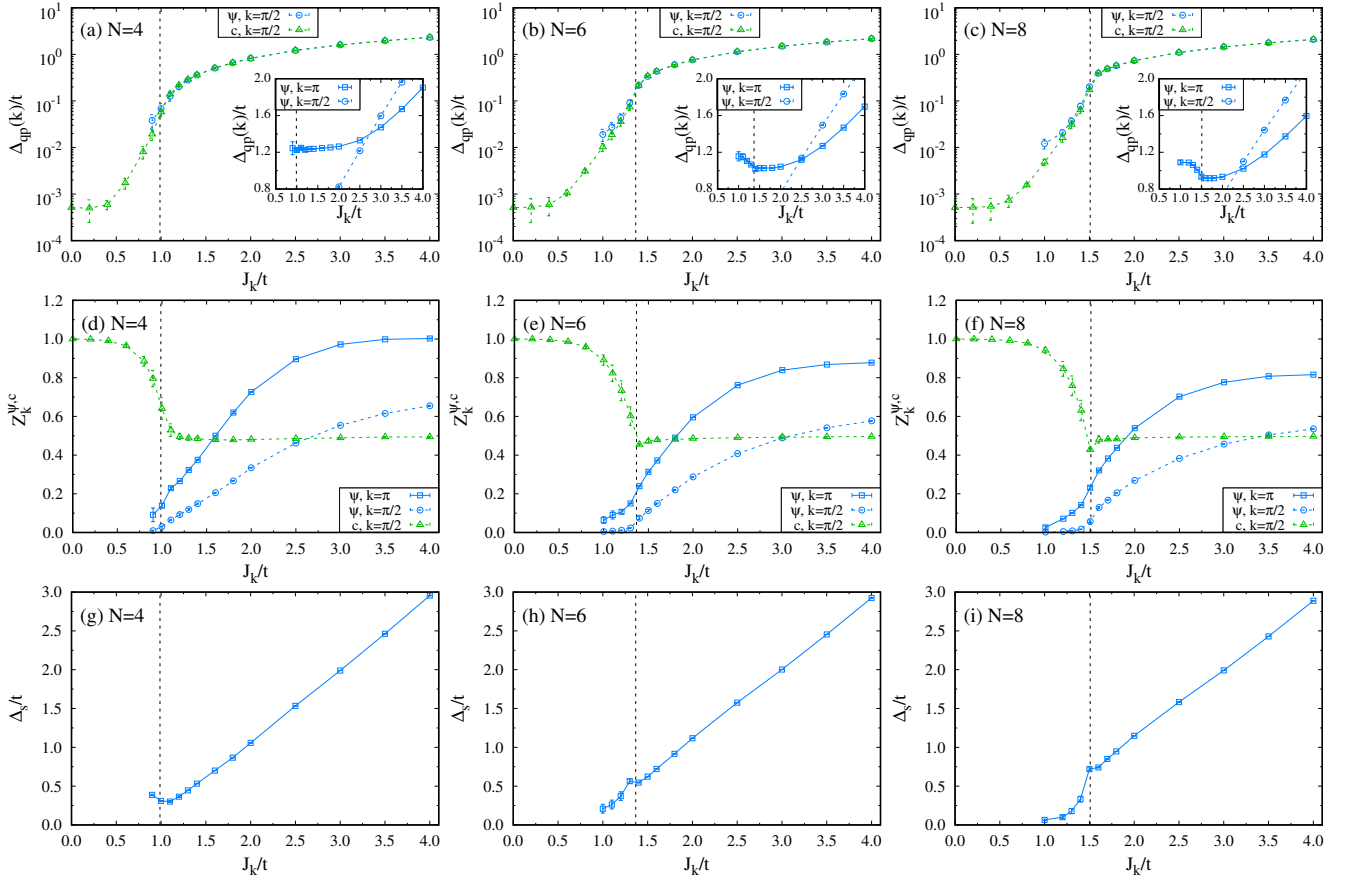


FIG. 15. (a)-(c) Single particle gap  $\Delta_{qp}(\mathbf{k})$  at  $\mathbf{k} = \pi/2$  on a semilog scale and (d)-(f) quasiparticle residue  $Z_{\mathbf{k}}^{\psi}$  at  $\mathbf{k} = \pi/2$  and  $\mathbf{k} = \pi$  of the pole in the composite fermion Green's function as a function of  $J_k/t$  in the  $SU(N)$  Kondo-Heisenberg chain with  $J_h/t = 1$ . Insets show a crossing between the quasiparticle gaps at  $\mathbf{k} = \pi/2$  and  $\mathbf{k} = \pi$ . To show an exponentially small gap at  $\mathbf{k} = \pi/2$  in the BOW phase of the  $c$  electron layer, we also plot  $\Delta_{qp}(\mathbf{k})$  with the corresponding residue  $Z_{\mathbf{k}}^c$  extracted from the conduction electron Green's function. Panels (g)-(i) show the evolution of the spin gap  $\Delta_s(\mathbf{q})$  at  $\mathbf{q} = \pi$  from the imaginary time (total) spin correlation function. All the quantities are representative of the thermodynamic limit. Dashed lines indicate the respective critical Kondo couplings.

ite fermion  $G_{\psi}(\mathbf{k}, \tau)$  and conduction electron  $G_c(\mathbf{k}, \tau)$  Green's functions. In the presence of Kondo screening they shall display the same asymptotic behavior, and indeed, a good data match is obtained (note the semilog scale) in the vicinity of  $J_k^c$ . However, a growing discrepancy occurs upon going deeper into the ordered phase where the low intensity of the composite quasiparticle [circles in Fig. 15(d)-15(f)] makes the analysis more difficult. Therefore, we are left with the conduction electron data which are consistent with an exponentially small gap. Thus accordingly larger systems sizes are indispensable to reliably track the onset of the gap at smaller values of  $J_k/t$ .

To locate the change in the position of the minimal quasiparticle gap as a function of  $J_k/t$ , we have equally extracted the single particle gap at  $\mathbf{k} = \pi$ . As shown in the insets of Figs. 15(a)-15(c), the gap at  $\mathbf{k} = \pi/2$  grows faster and eventually surpasses the one at  $\mathbf{k} = \pi$  bringing the electronic structure in line with that of a pure Kondo chain. We also note the hardening of the

gap at  $\mathbf{k} = \pi$  on the ordered side of  $J_k^c$ . We attribute it to the combined effect of dimerization and the persistence of Kondo screening. The latter gives rise to a smooth evolution of composite fermion residue  $Z_{\mathbf{k}=\pi}^{\psi}$  [squares in Figs. 15(d)-15(f)] across the phase transition for each value of  $N$ . In contrast, the evolution of conduction electron residue  $Z_{\mathbf{k}=\pi/2}^c$  [triangles in Figs. 15(d)-15(f)] across  $J_k^c$  is highly nontrivial. On the one hand, it quickly saturates for  $J_k > J_k^c$  at  $1/2$  implying the equal distribution of spectral weight between the two bands of the Kondo insulator. In the  $J_k = 0$  limit, it reaches the value of unity as expected for the free electron gas. On the other hand, for  $N > 4$  the data quality allows us to resolve a small drop in  $Z_{\mathbf{k}=\pi/2}^c$  in the vicinity of  $J_k^c$  on the ordered side. It is consistent with the redistribution of spectral weight so as to reflect the emergent four band structure, cf. Fig. 10(g). This effect is quickly masked by the overall growth of the  $c$  electron weight driven by the weakening of Kondo screening.

Finally, Figs. 15(g)-15(i) plot the evolution of spin gap



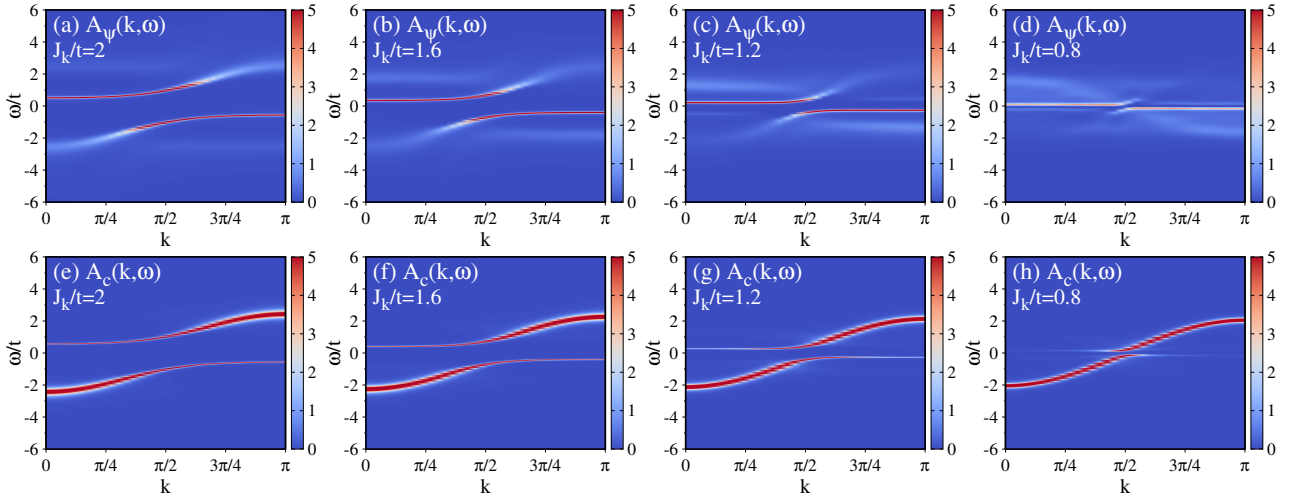


FIG. 16. (a)-(d) Composite fermion  $A_\psi(\mathbf{k}, \omega)$  and (e)-(h) conduction electron  $A_c(\mathbf{k}, \omega)$  spectral functions of the bare ( $J_h = 0$ )  $L = 66$   $SU(4)$  Kondo chain for selected values of  $J_k/t$ . The ground state in all panels corresponds to a uniform Kondo insulator.

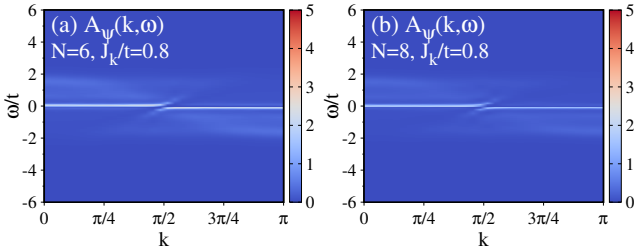


FIG. 17. Composite fermion  $A_\psi(\mathbf{k}, \omega)$  spectral function of the  $L = 66$  (a)  $SU(6)$  and (b)  $SU(8)$  Kondo chain with  $J_k/t = 0.8$ .

$\Delta_s(\mathbf{q} = \pi)$  obtained from the asymptotic behavior for large  $\tau t \gg 1$  of the imaginary time spin-spin correlation function  $S(\mathbf{q}, \tau) \propto e^{-\Delta_s(\mathbf{q})\tau}$ . As is evident, the spin gap in the disordered phase scales as  $J_k$  including the  $N = 4$  case with a relatively small  $J_k^c/t \simeq 1$ . This linear behavior indicates that the assumed Heisenberg coupling  $J_h/t = 1$  automatically places the system in the strong coupling limit  $J_k/t \gg 1$  of the bare Kondo chain where  $\Delta_s \propto J_k$  [43]. Notably, the critical coupling  $J_k^c$  seems to be marked by a weak dip. The latter is superseded by a rapid softening of  $\Delta_s$  in the ordered phase. These findings are in accord with the observed smearing of the triplon mode in the  $SU(8)$  spin excitation spectrum, see Figs. 14(b) versus 14(c).

## B. $SU(N)$ Kondo chain

Having explored the physics of the  $SU(N)$  Kondo-Heisenberg model, we turn now to a pure ( $J_h = 0$ )  $SU(N)$  Kondo chain. Given that already the  $SU(4)$  spin rotational symmetry of the Heisenberg chain is sufficient to stabilize a dimerized ground state [76, 77], the key question to address is whether the bare  $SU(N)$  Kondo chain

spontaneously dimerizes too, i.e., can the low dimensionality of the RKKY interaction alone produce long range dimer order?

On the one hand, in Sec. III A we found that the critical magnetic interaction required to trigger dimer order in the  $SU(4)$  Kondo-Heisenberg chain seems to scale linearly with  $J_k$ . Since the RKKY interaction scales for small Kondo couplings as  $\frac{J_k^2}{N}$  [35], one may anticipate the absence of dimer order in the  $SU(4)$  Kondo chain. On the other hand, a higher symmetry of fermion flavors shifts the critical Kondo coupling  $J_k^c$  to larger values and increases the domain of stability of the VBS phase, see the phase diagram in Fig. 3. Thus, the question of a spontaneous dimerization still remains an open issue in a generic  $SU(N)$  case.

We begin our study with the evolution of composite fermion  $A_\psi(\mathbf{k}, \omega)$  and conduction electron  $A_c(\mathbf{k}, \omega)$  spectral functions of the  $SU(4)$  Kondo chain shown in Fig. 16. While the main spectral features are quantitatively reproduced within a simple large- $N$  approximation accounting for Kondo screening in the translationally invariant Kondo chain, see Fig. 1, one observes that extra features in  $A_\psi(\mathbf{k}, \omega)$ , i.e., shadow bands become more pronounced at small values of  $J_k/t$ . As argued in Ref. [36], they reflect antiferromagnetic spin fluctuations driven by the RKKY interaction, and they correspond to the image of the  $c$  electron spectral function shifted by the antiferromagnetic wavevector  $\mathbf{Q} = \pi$ . Since the RKKY energy scale is suppressed as  $1/N$ , the shadow bands shall lose their intensity with increasing  $N$  bringing the overall spectrum, in the absence of enhanced spin dimer correlations, in line with the large- $N$  outcome in Fig. 1. We confirm this point explicitly in Fig. 17 by plotting  $A_\psi(\mathbf{k}, \omega)$  at our smallest value  $J_k/t = 0.8$  for the  $N = 6$  and  $N = 8$  case. The apparent similarity between the QMC data and the corresponding large- $N$  result in Fig. 1(d) suggests the absence of significant dimer-dimer correlations.

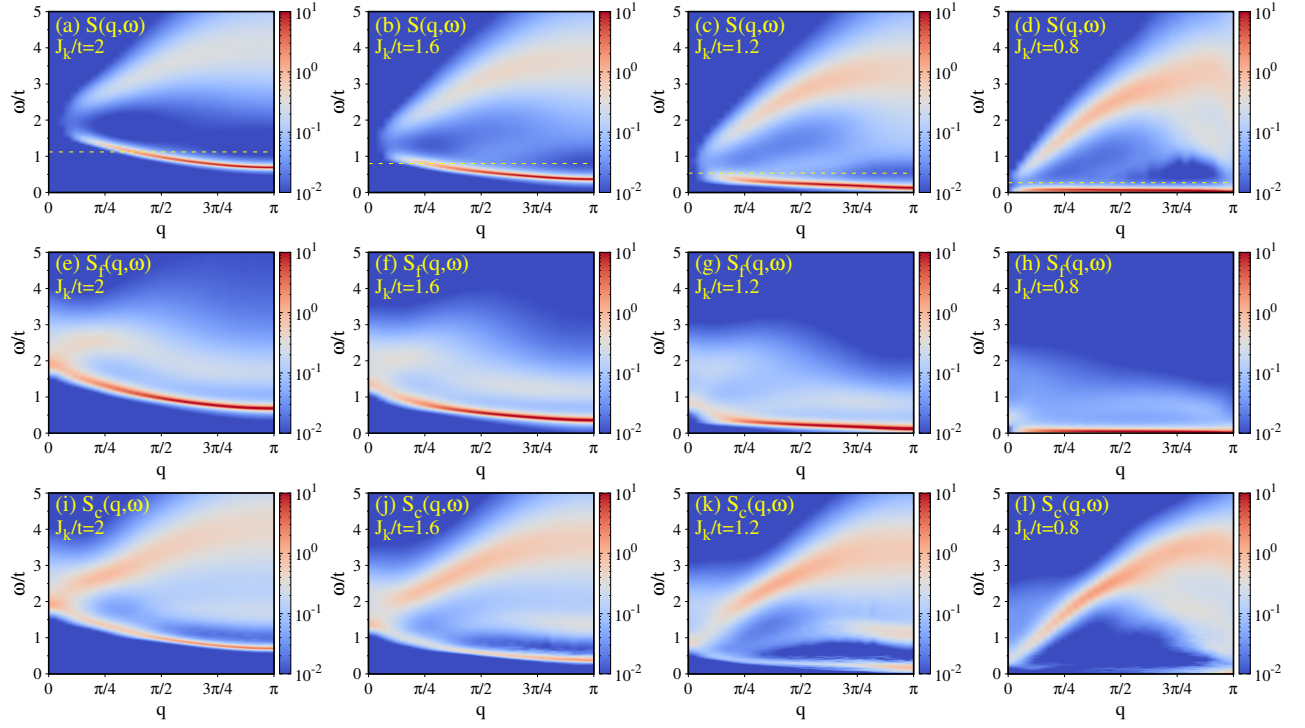


FIG. 18. Dynamical spin structure factor of the  $L = 66$   $SU(4)$  Kondo chain for: (a)-(d) total spin  $S(\mathbf{q}, \omega)$ ; (e)-(h)  $f$  spin  $S_f(\mathbf{q}, \omega)$ , and (i)-(l) conduction electron spin  $S_c(\mathbf{q}, \omega)$ . Dashed lines indicate the particle-hole continuum threshold. Parameters as in Fig. 16.

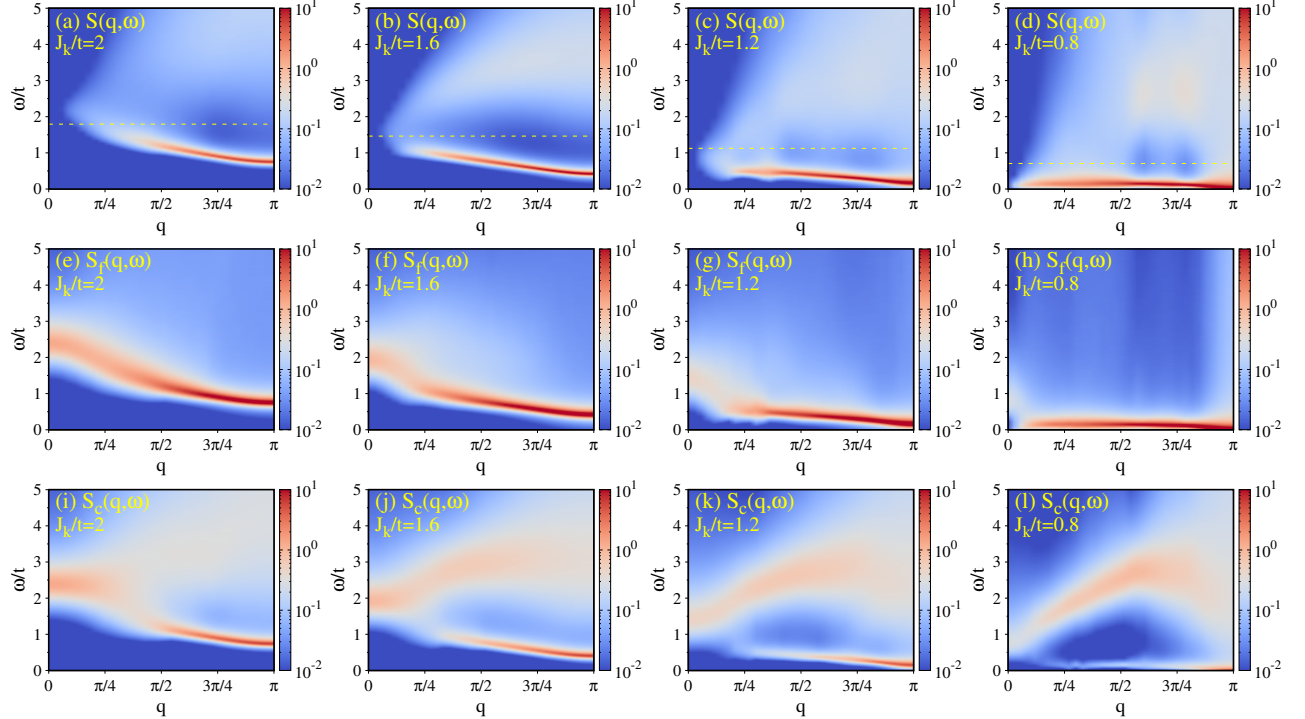


FIG. 19. Same as in Fig. 18 but for the  $SU(2)$  Kondo chain.

To complement our analysis of dynamical properties of the  $SU(4)$  Kondo chain, we plot in Fig. 18 the cor-

responding spin excitation spectra. Irrespective of the value of  $J_k/t$ , the dynamical spin structure factor  $S(\mathbf{q}, \omega)$

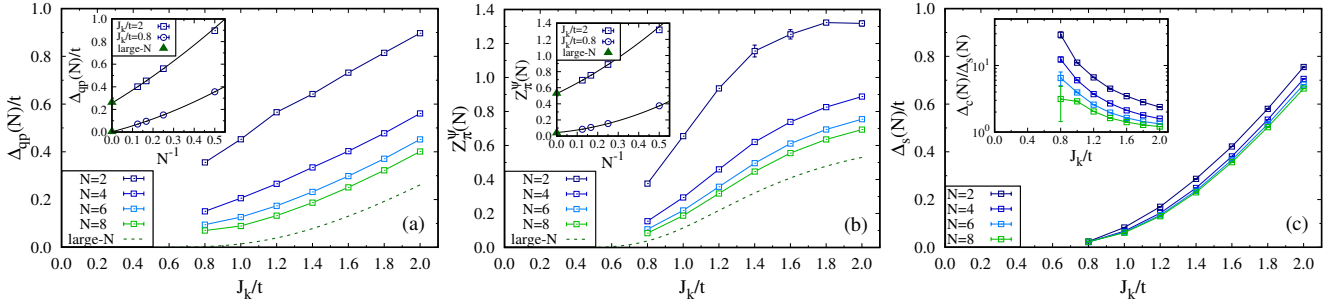


FIG. 20. (a) Single particle gap  $\Delta_{qp}(N)$  at  $\mathbf{k} = \pi$  and (b) the corresponding residue  $Z_{\mathbf{k}=\pi}^{\psi}(N)$  of the pole in the composite fermion Green's function as a function of  $J_k/t$  in the  $SU(N)$  Kondo chain. Dashed lines correspond to the large- $N$  value of  $\Delta_{qp}$  and  $Z_{\mathbf{k}=\pi}^{\psi}$ . Insets show second order polynomial fits to the QMC data at  $J_k/t = 2$  and  $J_k/t = 0.8$  to extract the quasiparticle gap and residue in the  $N \rightarrow \infty$  limit. Within error bars, the latter match the large- $N$  values (triangles). Panel (c) shows the evolution of the spin gap  $\Delta_s(N)$  at  $\mathbf{q} = \pi$  extracted from the imaginary time displaced (total) spin correlation function and the inset shows the ratio between the charge  $\Delta_c(N) = 2\Delta_{qp}(N)$  and spin gap on a semilog scale. All the quantities have been extrapolated to the thermodynamic limit, see Appendix 2.

displays the same main spectral features: (i) a low energy triplon mode with a minimal gap at the antiferromagnetic wavevector  $\mathbf{Q} = \pi$ , and (ii) particle-hole excitations of nearly free conduction electrons above the charge gap, see Figs. 18(a)-18(d).

As is apparent, Kondo screening unites the individual dynamics of the local  $f$  and conduction electron spins such that both  $S_f(\mathbf{q}, \omega)$  and  $S_c(\mathbf{q}, \omega)$  spectra have the same support but differ in terms of the distribution of spectral intensity. In fact, the dynamical coupling between local and itinerant spin degrees of freedom is not restricted to the lowest energy triplon mode but the fingerprint of the particle-hole continuum in  $S_f(\mathbf{q}, \omega)$  extends over higher frequencies matching the energy window where sharp composite fermion bands occur in  $A_{\psi}(\mathbf{k}, \omega)$ , see Figs. 16(a)-16(d).

The observed flattening of the triplon mode for small  $J_k/t$  stems from the slowing down of the spin velocity  $v_s$  determined by the effective RKKY coupling  $J_{\text{RKKY}} \propto \frac{J_k^2}{N}$ . While the occurrence of the triplon mode induces the rearrangement of spectral intensity distribution in the particle-hole continuum, an extremely soft flat triplon in Fig. 18(d) is found below the charge gap across the whole Brillouin zone. It allows one to reveal a typical free-electron-like continuum delimited around  $\mathbf{q} = \pi$  by a lower and upper boundary. The latter carries most of the spectral weight and hence the overall form of both  $S(\mathbf{q}, \omega)$  and  $S_c(\mathbf{q}, \omega)$  above the triplon mode can be well approximated using a convolution of the single particle Green's function, i.e., particle-hole "bubble" diagram.

Anticipating that the validity of the "bubble" diagram might be specific to the enhanced  $SU(4)$  spin symmetry of the model, we clarify this issue by plotting in Fig. 19 spin excitation spectra of the conventional  $SU(2)$  Kondo chain. As can be seen, spectral intensity in  $S(\mathbf{q}, \omega)$  does not rearrange so as to recover the free-electron-like continuum upon approaching the weak coupling, see Figs. 19(c) and 19(d). Moreover, the "bubble" diagram cannot account for a high frequency part of  $S_c(\mathbf{q}, \omega)$  with

the upper branch blurred close to  $\mathbf{q} = \pi$  into broad featureless excitations, see Fig. 19(1). These findings underscore the essential role of vertex correction effects in the spin dynamics of the  $SU(2)$  model.

Importantly, regardless of the number of fermion flavors and down to our smallest  $J_k/t = 0.8$ , we find no clear evidence of the two-spinon continuum in  $S_f(\mathbf{q}, \omega)$ , see Figs. 18(h) and 19(h), in contrast to the  $f$  spin dynamics of the  $SU(N)$  Kondo-Heisenberg chain shown in Figs. 13(h) and 14(h).

As for the triplon mode, a more pronounced piling up of the spectral weight at  $\mathbf{q} = \pi$  seen in  $S_c(\mathbf{q}, \omega)$  of the  $N = 2$  model, is consistent with a larger, with respect to the  $N = 4$  case, effective RKKY coupling  $J_{\text{RKKY}} \propto \frac{J_k^2}{N}$  producing stronger antiferromagnetic spin fluctuations.

Next, we examine the impact of an enlarged  $SU(N)$  symmetry of the model on reducing the separation of charge and spin energy scales specific to the KI state. To this end, we plot in Fig. 20 a single particle gap  $\Delta_{qp}(N, \mathbf{k})$  at  $\mathbf{k} = \pi$ , the corresponding quasiparticle residue  $Z_{\mathbf{k}}^{\psi}(N)$ , as well as the spin gap  $\Delta_s(N, \mathbf{q})$  at  $\mathbf{q} = \pi$  as a function of  $J_k/t$ . Following the same fitting procedure as in Sec. III A 6, we have extracted finite size estimates of these quantities from the asymptotic form of imaginary time composite fermion Green's  $G_{\psi}(\mathbf{k}, \tau)$  and spin-spin correlation  $S(\mathbf{q}, \tau)$  functions at large imaginary time  $\tau$ . The data in Fig. 20 correspond the thermodynamic limit based on QMC results on chains up to  $L = 130$  sites. As shown in Fig. 20(a), the  $N = 2$  quasiparticle gap clearly stands out and tracks  $J_k$  in the weak coupling limit. This behavior bears a striking similarity to a linear dependence of  $\Delta_{qp}$  in the magnetically ordered phase of the particle-hole symmetric 2D Kondo lattice model [19, 20, 29, 32, 34]. Long range antiferromagnetic order does not occur in one dimension resulting in a finite spin gap  $\Delta_s \propto e^{-t/J_k}$  in the weak coupling limit. This tiny gap inhibits reliable QMC simulations below  $J_k/t = 0.8$ : The extrapolated value of  $\Delta_s$  at  $J_k/t = 0.7$

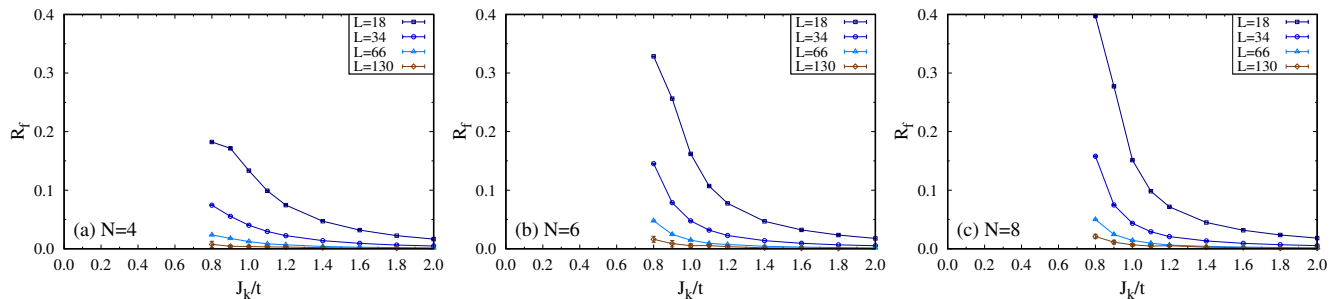


FIG. 21. Correlation ratio  $R_f$  from the structure factor of  $f$  spin dimer correlations in the bare  $SU(N)$  Kondo chain: (a)  $N = 4$ ; (b)  $N = 6$ , and (c)  $N = 8$ .

is not distinguishable within error bars from zero, spuriously indicating onset of long range magnetic order, see Appendix 2. Due to the exponentially small spin gap, the antiferromagnetic spin correlation length  $\xi_s \propto \frac{v_s}{\Delta_s}$  is much longer than the conduction electron coherence length  $\xi_c \propto \frac{t}{\Delta_{qp}}$ . As a consequence, the  $c$  electrons are effectively subject to a quasistatic staggered local moment which accounts for  $\Delta_{qp} \propto J_k$  as in the magnetically ordered phase [43]. The observed asymptotic reduction of  $\Delta_{qp}$  to its large- $N$  limit (dashed line) is driven by the vanishing of vertex corrections brought by the RKKY energy scale  $J_{\text{RKKY}} \propto \frac{J_k^2}{N}$ .

Furthermore, since the composite fermion operator directly provides the measure of hybridization,  $\hat{\psi}_{i,\sigma}^\dagger \propto \hat{f}_{i,\sigma}^\dagger V$  [36], one would expect the quasiparticle residue of the composite fermion  $Z_{\mathbf{k}}^\psi$  to track  $V^2 Z_{\mathbf{k}}^f$ , where  $Z_{\mathbf{k}}^f$  is a large- $N$  coherence factor in Eq. (20). However, as quantified in Fig. 20(b),  $Z_{\mathbf{k}=\pi}^\psi$  for the  $N = 2$  case does not follow the expected exponentially small Kondo scale of the large- $N$  approach (dashed line). Our data obtained in the absence of long range antiferromagnetic order indicate that the observed enhancement of spectral weight is unrelated to the Fermi surface nesting driven magnetism. Instead, we believe that it is an intrinsic property of the composite fermion operator in the presence of strong antiferromagnetic spin fluctuations [43–46].

Notably, we were able to recover within error bars the large- $N$  values of both the single particle gap and quasiparticle weight by extrapolating the QMC data at  $J_k/t = 2$  and  $J_k/t = 0.8$  to the  $N \rightarrow \infty$  limit, see the inset of Figs. 20(a) and 20(b), confirming that the large- $N$  theory is a correct saddle point of the  $SU(2)$  Kondo chain. In addition, to quantify the strength of correlation effects in the KI state using a single measure [129], we plot in the inset of Fig. 20(c) the ratio between the charge gap  $\Delta_c = 2\Delta_{qp}$  and the spin gap  $\Delta_s$ . As is evident, up to our largest value of  $N = 8$  this quantity is always larger than 1 and gets strongly enhanced in the weak-coupling limit. It marks a difference with respect to a conventional band insulator where the trivial splitting between bonding and antibonding bands produces identical charge and spin excitation gaps [47, 48].

Finally, in order to directly confirm that the enlarged  $SU(N)$  symmetry of the RKKY interaction does not lead to the enhancement of staggered valence bond fluctuations, we plot in Fig. 21 the correlation ratio  $R_f$  given by Eq. (25). Even though larger  $N$  leads on our shortest  $L = 18$  chain to a systematic increase of  $R_f$  in the small  $J_k/t$  region, the observed *downscaling* of  $R_f$  for increasingly larger system sizes implies the translational invariance of the ground state in the thermodynamic limit.

#### IV. SUMMARY AND OUTLOOK

The main motivation of this work was to investigate dynamical signatures of the formation of VBS order and its interplay with Kondo screening in a model system accessible to sign free QMC simulations. For this reason, we have considered a 1D  $SU(N)$  Kondo-Heisenberg lattice model in the fully antisymmetric self-adjoint representation. We have been able to determine the phase diagram for the case of a half-filled conduction electron band, and we showed that in the  $N \geq 4$  case there is a quantum phase transition between the Kondo insulating phase and the VBS/BOW state, which is in the universality class of the 2D classical Ising model.

While making a definite statement about Kondo breakdown at small Kondo couplings  $J_k/t$  within the dimerized phase would require us to simulate exponentially large lattices, our data extend the list of known examples (albeit with magnetic order) where the order-disorder transition and the breakdown of heavy quasiparticles defined by the loss of a pole in the composite fermion Green's function are detached. Thus, the coexistence of Kondo screening and long range order is not restricted to spontaneous breaking of a continuous  $SU(N)$  spin rotational symmetry of the Hamiltonian and to the resultant emergence of Goldstone bosons (spin waves), but it also happens in the case of discrete (translational) symmetry breaking by long range dimer correlations.

The  $U(1)$  gauge theory formulation of the Kondo lattice model in Sec. II, introduces three particles, the bare fermion,  $\hat{c}_{i,\sigma}^\dagger$ , the composite fermion,  $\hat{\Psi}_{i,\sigma}^\dagger$ , as well as the gauge fermion,  $\hat{f}_{i,\sigma}^\dagger$ . The bare fermion and the composite

fermion have the quantum number of the electron: globally conserved charge and spin. The  $f$  fermion carries a locally conserved gauge charge and globally conserved spin degrees of freedom but no electric charge. The composite and bare fermions can delocalize, and both will participate in the Luttinger count. On the other hand, the  $f$  fermions cannot hybridize with the conduction electrons and composite fermions due to the mismatch of quantum numbers. In Monte Carlo simulations, we can investigate the dynamics of the bare and composite fermions by computing the corresponding spectral function. In contrast, understanding the dynamics of the  $f$  fermions is more delicate since the single particle propagation involves a gauge string. We can, however, extract the dynamical spin structure factor  $S_f(\mathbf{q}, \omega)$  for the  $f$  spins and by comparing it to that of the isolated  $SU(N)$  Heisenberg chain, we can assess if the  $f$  fermions are present as possibly *fractionalized* particles in one part of the spectrum.

Let us now interpret aspects of our data in terms of the above, and concentrate on the  $SU(4)$  case. The Kondo screened phase at large  $J_k/t = 4$  can be understood solely in terms of the hybridization of the composite and bare electrons, see Figs. 9(a) and 9(e). The triplon mode observed in the spin dynamical structure factor can be well accounted for by considering vertex corrections to the particle-hole excitations that form a bound state below the particle-hole continuum, see Figs. 13(a), 13(e), and 13(i). At our smallest value of  $J_k/t = 0.8$  in the VBS/BOW phase, the situation is more complicated and better understood by taking the limit of a Kondo breakdown. That is, solely in terms of the  $f$  fermions and  $c$  electrons. The dynamical spectral function of the  $f$  fermions in Fig. 13(h) shows a dimerization gap and, above it, a continuum. On the one hand, the similarity to the pure  $SU(4)$  Heisenberg chain in Fig. 12(b) is very evident and suggests the interpretation in terms of a two-spinon continuum. On the other hand, given that the charge gap at  $J_k/t = 0.8$  is lower than the dominant features, one could argue that one cannot really distinguish between Landau damping and spinons. However, owing to the different quantum numbers of the  $f$  fermions and  $c$  electrons, the two-spinon continuum cannot couple to the particle-hole continuum of the conduction electrons. This line of arguing supports our discussion in Sec. III A based on the presence of fractionalized particles. Furthermore, a nonvanishing local spin-spin correlation function  $S_{cf}$  in Fig. 8 implies an ultraviolet coupling between the spin chain and conduction electrons. Clearly, since the spin chain dimerizes, the conduction electrons will be subject to a dimerization potential. As a consequence, a gap opens at  $\mathbf{k} = \pi/2$  in the conduction electron spectral function and backfolding of the band is apparent in Fig. 9(h).

We can contrast the above results with those in Sec. III B for the bare  $SU(4)$  Kondo chain which hosts solely the Kondo insulating phase. As a consequence of the hybridization of the composite and bare fermions, the

spin excitation spectrum displays a more conventional structure with the low energy triplon mode and particle-hole excitations of nearly free conduction electrons above the charge gap, see Fig. 18.

The starting point of our study corresponds to a dimerized ground state of the  $SU(N)$  Heisenberg chain. A complementary avenue is to consider an  $SU(N)$  Kondo-Hubbard chain with an additional Hubbard interaction between the conduction electrons: In the limit  $J_k = 0$ , there is evidence that a pure  $SU(N > 2)$  Hubbard chain at half filling hosts a dimerized ground state [130–132]. Introducing Kondo coupling  $J_k$  to a lattice of magnetic impurities provides another possibility to study the effect of quantum critical dimer fluctuations on Kondo screening.

Along these lines, an enlarged symmetry of fermion flavors can pave the way to study the interplay of VBS order and Kondo screening in higher dimensions: It is known that the  $SU(6)$  Hubbard model on the square lattice exhibits at  $U/t \simeq 13.3$  a phase transition between long range antiferromagnetic order and a VBS state [133]. Hence, of particular interest is the question of what happens in the vicinity of this quantum critical point in the presence of finite Kondo coupling  $J_k$ . Indeed, in the parameter range where Kondo screening, magnetism, and VBS order strongly compete, solutions with larger unit cells, e.g., Kondo stripes [134, 135] are conceivable. We hope to address these new research directions in the near future.

## ACKNOWLEDGMENTS

The authors gratefully acknowledge the Gauss Centre for Supercomputing e.V. (www.gauss-centre.eu) for funding this project by providing computing time through the John von Neumann Institute for Computing (NIC) on the GCS Supercomputer JUWELS [136] at Jülich Supercomputing Centre (JSC). M.R. is funded by the Deutsche Forschungsgemeinschaft (DFG, German Research Foundation), Project No. 332790403. F.F.A. acknowledges financial support from the DFG under the grant AS 120/16-1 (Project No. 493886309) that is part of the collaborative research project SFB Q-M&S funded by the Austrian Science Fund (FWF) F 86 as well as the Würzburg-Dresden Cluster of Excellence on Complexity and Topology in Quantum Matter ct.qmat (EXC 2147, Project No. 390858490).

## Appendix: Supplemental QMC data

Here we provide further details about the QMC simulation results discussed in the main text.

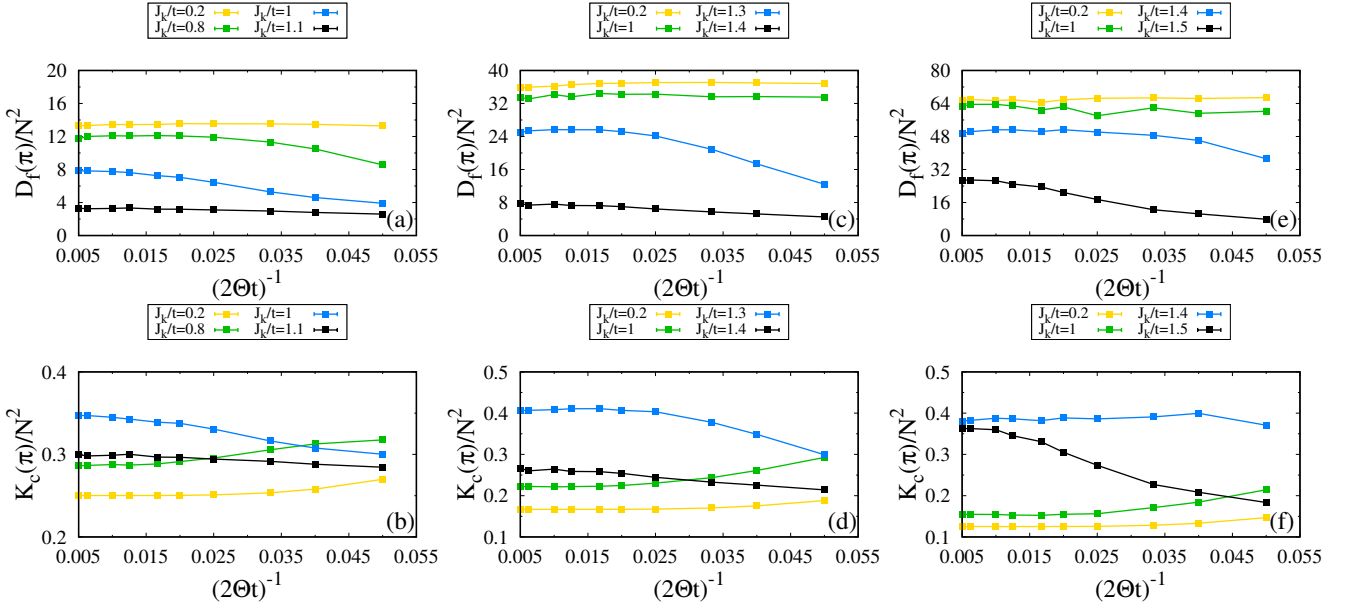


FIG. 22. Convergence of the  $f$  spin dimer  $D_f(\mathbf{q} = \pi)/N^2$  (top) and kinetic energy dimer  $K_c(\mathbf{q} = \pi)/N^2$  (bottom) structure factors at representative values of  $J_k/t$  as a function of the projection parameter  $\Theta t$  for the  $L = 66$   $SU(N)$  Kondo-Heisenberg chain with  $J_h/t = 1$ : (a),(b)  $N = 4$ ; (c),(d)  $N = 6$ , and (e),(f)  $N = 8$ .

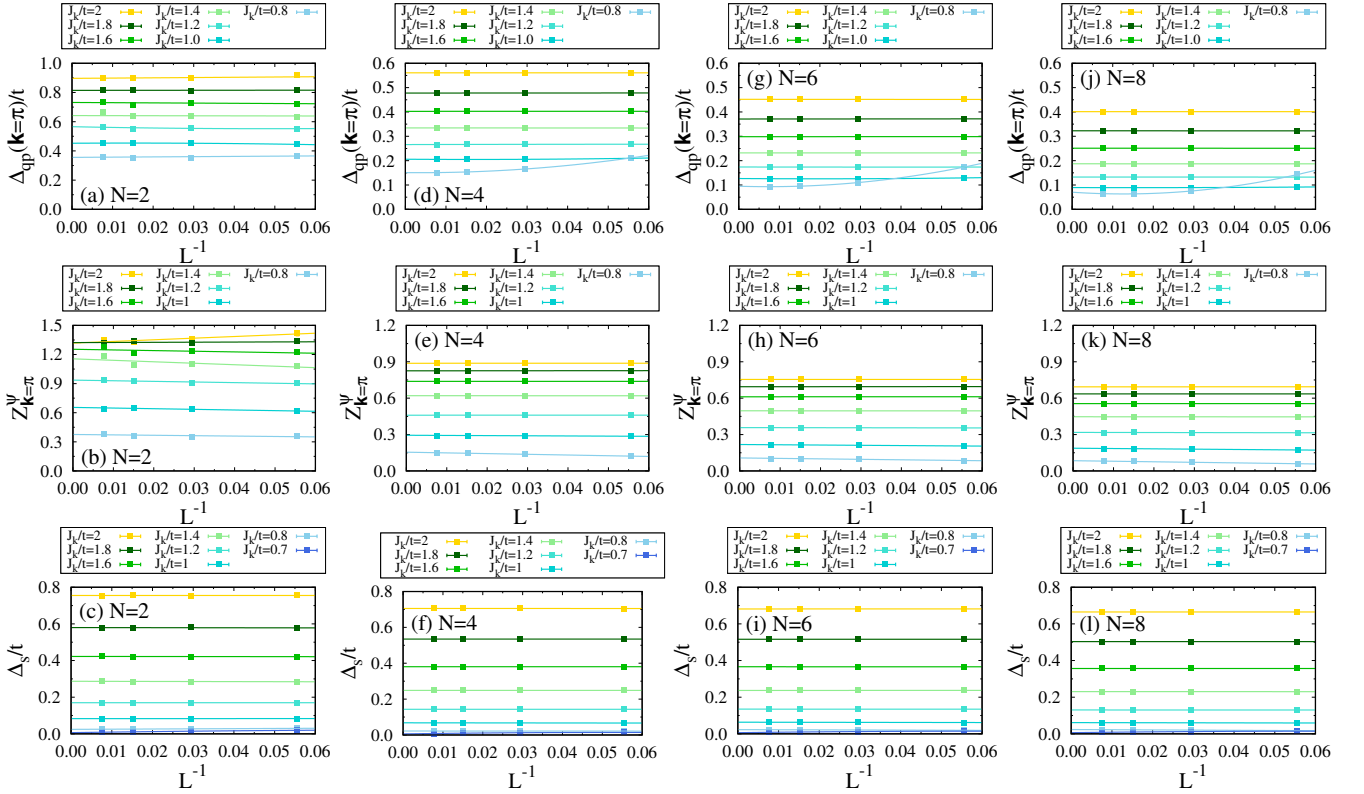


FIG. 23. Finite size extrapolation of the single particle gap  $\Delta_{qp}$  at  $\mathbf{k} = \pi$  (top), the corresponding residue  $Z_{\mathbf{k}=\pi}^{\psi}$  (middle) of the pole in the composite fermion Green's function, and the spin gap  $\Delta_s$  at  $\mathbf{q} = \pi$  (bottom) for representative values of  $J_k/t$  in the  $SU(N)$  Kondo chain. Solid lines are linear and quadratic polynomial fits to the QMC data: (a)-(c)  $N = 2$ ; (d)-(f)  $N = 4$ ; (g)-(i)  $N = 6$ , and (j)-(l)  $N = 8$ . At  $J_k/t = 0.7$ , the extrapolated value of  $\Delta_s$  is not distinguishable within error bars from zero.

### 1. Effect of a finite projection parameter $\Theta$

In the adopted projective version of the QMC algorithm, the expectation value of a physical observable op-

erator  $\hat{O}$  is obtained using

$$\frac{\langle \Psi_0 | \hat{O} | \Psi_0 \rangle}{\langle \Psi_0 | \Psi_0 \rangle} = \lim_{\Theta \rightarrow \infty} \frac{\langle \Psi_T | e^{-\Theta \hat{H}} \hat{O} e^{-\Theta \hat{H}} | \Psi_T \rangle}{\langle \Psi_T | e^{-2\Theta \hat{H}} | \Psi_T \rangle} \quad (\text{A.1})$$

where  $|\Psi_0\rangle$  is the ground state and  $\Theta$  is a projection parameter chosen to be large enough to ensure that the trial wave function  $|\Psi_T\rangle$  is projected to the ground state. In practice, the ground state expectation value of the observable is obtained by searching for its convergent behavior as a function of  $\Theta$ . We illustrate this in Fig. 22 which plots  $f$  spin dimer  $D_f(\mathbf{q} = \pi)$  and kinetic energy dimer  $K_c(\mathbf{q} = \pi)$  structure factors from QMC simulations of the  $L = 66$   $SU(N)$  Kondo-Heisenberg chain for representative values of Kondo coupling  $J_k/t$ . From these plots, we find that  $2\Theta t = 40$  is sufficient in most cases to guarantee convergence of both quantities except for the quantum critical region where the ground state projection is slower and requires up to  $2\Theta t = 200$ . Thus, the data for  $K_c(\mathbf{q} = \pi)$  clarify that the weakening of bond order wave fluctuations in the valence bond solid phase, see Fig. 7 of the main text, is not an artifact of the finite

value of  $\Theta$  but it rather stems from the finite size.

## 2. Finite size scaling

Figure 23 shows examples of finite size scaling of the single particle gap  $\Delta_{qp}$  at  $\mathbf{k} = \pi$ , the corresponding residue  $Z_{\mathbf{k}=\pi}^\psi$  of the pole in the composite fermion Green's function, and the spin gap  $\Delta_s$  at  $\mathbf{q} = \pi$  in the  $SU(N)$  Kondo chain. Based on these scalings, we restricted our analysis in Sec. IIIB to  $J_k/t \geq 0.8$ : The extrapolated value of  $\Delta_s$  at  $J_k/t = 0.7$  is not distinguishable within error bars from zero, spuriously indicating the onset of long range magnetic order. Thus, properly addressing the weak coupling limit requires the simulation of chains with more than  $L = 130$  sites used in our study. The scaling results led us to Fig. 20 in the main text.

- 
- <sup>1</sup> S. Doniach, *The Kondo lattice and weak antiferromagnetism*, *Physica B+C* **91**, 231 (1977).
- <sup>2</sup> N. Tsukahara, S. Shiraki, S. Itou, N. Ohta, N. Takagi, and M. Kawai, *Evolution of Kondo Resonance from a Single Impurity Molecule to the Two-Dimensional Lattice*, *Phys. Rev. Lett.* **106**, 187201 (2011).
- <sup>3</sup> M. Raczkowski and F. F. Assaad, *Emergent Coherent Lattice Behavior in Kondo Nanosystems*, *Phys. Rev. Lett.* **122**, 097203 (2019).
- <sup>4</sup> J. Figgins, L. S. Mattos, W. Mar, Y.-T. Chen, H. C. Manoharan, and D. K. Morr, *Quantum engineered Kondo lattices*, *Nat. Commun.* **10**, 5588 (2019).
- <sup>5</sup> W. Wan, R. Harsh, A. Meninno, P. Dreher, S. Sajan, H. Guo, I. Errea, F. de Juan, and M. M. Ugeda, *Evidence for ground state coherence in a two-dimensional Kondo lattice*, *Nat. Commun.* **14**, 7005 (2023).
- <sup>6</sup> M. Oshikawa, *Topological Approach to Luttinger's Theorem and the Fermi Surface of a Kondo Lattice*, *Phys. Rev. Lett.* **84**, 3370 (2000).
- <sup>7</sup> P. Coleman, C. Pépin, Q. Si, and R. Ramazashvili, *How do Fermi liquids get heavy and die?* *J. Phys.: Condens. Matter* **13**, R723 (2001).
- <sup>8</sup> Q. Si, S. Rabello, K. Ingersent, and J. L. Smith, *Locally critical quantum phase transitions in strongly correlated metals*, *Nature (London)* **413**, 804 (2001).
- <sup>9</sup> B. Danu, M. Vojta, F. F. Assaad, and T. Grover, *Kondo Breakdown in a Spin-1/2 Chain of Adatoms on a Dirac Semimetal*, *Phys. Rev. Lett.* **125**, 206602 (2020).
- <sup>10</sup> M. Raczkowski, B. Danu, and F. F. Assaad, *Breakdown of heavy quasiparticles in a honeycomb Kondo lattice: A quantum Monte Carlo study*, *Phys. Rev. B* **106**, L161115 (2022).
- <sup>11</sup> A. Gleis, J.-W. Li, and J. von Delft, *Controlled Bond Expansion for Density Matrix Renormalization Group Ground State Search at Single-Site Costs*, *Phys. Rev. Lett.* **130**, 246402 (2023).
- <sup>12</sup> M. Vojta, *Orbital-Selective Mott Transitions: Heavy Fermions and Beyond*, *J. Low Temp. Phys.* **161**, 203 (2010).
- <sup>13</sup> A. Gleis, S.-S. B. Lee, G. Kotliar, and J. von Delft, *Emergent Properties of the Periodic Anderson Model: a High-Resolution, Real-Frequency Study of Heavy-Fermion Quantum Criticality*, [arXiv:2310.12672](https://arxiv.org/abs/2310.12672) (2023).
- <sup>14</sup> F. Eickhoff and F. B. Anders, *Kondo breakdown in multi-orbital Anderson lattices induced by destructive hybridization interference*, [arXiv:2401.04540](https://arxiv.org/abs/2401.04540) (2024).
- <sup>15</sup> H. v. Löhneysen, A. Rosch, M. Vojta, and P. Wölfle, *Fermi-liquid instabilities at magnetic quantum phase transitions*, *Rev. Mod. Phys.* **79**, 1015 (2007).
- <sup>16</sup> P. Gegenwart, Q. Si, and F. Steglich, *Quantum criticality in heavy-fermion metals*, *Nat. Phys.* **4**, 186 (2008).
- <sup>17</sup> Q. Si and F. Steglich, *Heavy Fermions and Quantum Phase Transitions*, *Science* **329**, 1161 (2010).
- <sup>18</sup> Z.-P. Shi, R. R. P. Singh, M. P. Gelfand, and Z. Wang, *Phase transitions in the symmetric Kondo-lattice model in two and three dimensions*, *Phys. Rev. B* **51**, 15630 (1995).
- <sup>19</sup> F. F. Assaad, *Quantum Monte Carlo Simulations of the Half-Filled Two-Dimensional Kondo Lattice Model*, *Phys. Rev. Lett.* **83**, 796 (1999).
- <sup>20</sup> S. Capponi and F. F. Assaad, *Spin and charge dynamics of the ferromagnetic and antiferromagnetic two-dimensional half-filled Kondo lattice model*, *Phys. Rev. B* **63**, 155114 (2001).
- <sup>21</sup> M. Feldbacher, C. Jurecka, F. F. Assaad, and W. Brenig, *Single-hole dynamics in the half-filled two-dimensional Kondo-Hubbard model*, *Phys. Rev. B* **66**, 045103 (2002).
- <sup>22</sup> W. Zheng and J. Oitmaa, *Zero-temperature series expansions for the Kondo lattice model at half filling*, *Phys. Rev. B* **67**, 214406 (2003).
- <sup>23</sup> T. Senthil, M. Vojta, and S. Sachdev, *Weak magnetism and non-Fermi liquids near heavy-fermion critical points*, *Phys. Rev. B* **69**, 035111 (2004).
- <sup>24</sup> H. Watanabe and M. Ogata, *Fermi-Surface Reconstruction without Breakdown of Kondo Screening at the Quantum Critical Point*, *Phys. Rev. Lett.* **99**, 136401 (2007).
- <sup>25</sup> L. C. Martin and F. F. Assaad, *Evolution of the Fermi Surface across a Magnetic Order-Disorder Transition in the Two-Dimensional Kondo Lattice Model: A Dynamical Cluster Approach*, *Phys. Rev. Lett.* **101**, 066404 (2008).
- <sup>26</sup> N. Lanatà, P. Barone, and M. Fabrizio, *Fermi-surface evolution across the magnetic phase transition in the Kondo lattice model*, *Phys. Rev. B* **78**, 155127 (2008).

- <sup>27</sup> M. Vojta, *From itinerant to local-moment antiferromagnetism in Kondo lattices: Adiabatic continuity versus quantum phase transitions*, *Phys. Rev. B* **78**, 125109 (2008).
- <sup>28</sup> J. Otsuki, H. Kusunose, and Y. Kuramoto, *Evolution of a Large Fermi Surface in the Kondo Lattice*, *Phys. Rev. Lett.* **102**, 017202 (2009).
- <sup>29</sup> L. C. Martin, M. Bercx, and F. F. Assaad, *Fermi surface topology of the two-dimensional Kondo lattice model: Dynamical cluster approximation approach*, *Phys. Rev. B* **82**, 245105 (2010).
- <sup>30</sup> M. Z. Asadzadeh, F. Becca, and M. Fabrizio, *Variational Monte Carlo approach to the two-dimensional Kondo lattice model*, *Phys. Rev. B* **87**, 205144 (2013).
- <sup>31</sup> R. Peters and N. Kawakami, *Large and small Fermi-surface spin density waves in the Kondo lattice model*, *Phys. Rev. B* **92**, 075103 (2015).
- <sup>32</sup> B. Lenz, R. Gezzi, and S. R. Manmana, *Variational cluster approach to superconductivity and magnetism in the Kondo lattice model*, *Phys. Rev. B* **96**, 155119 (2017).
- <sup>33</sup> J. P. L. Faye, M. N. Kiselev, P. Ram, B. Kumar, and D. Sénéchal, *Phase diagram of the Hubbard-Kondo lattice model from the variational cluster approximation*, *Phys. Rev. B* **97**, 235151 (2018).
- <sup>34</sup> R. Eder and P. Wróbel, *Antiferromagnetic phase of the Kondo insulator*, *Phys. Rev. B* **98**, 245125 (2018).
- <sup>35</sup> M. Raczkowski and F. F. Assaad, *Phase diagram and dynamics of the SU(N) symmetric Kondo lattice model*, *Phys. Rev. Research* **2**, 013276 (2020).
- <sup>36</sup> B. Danu, Z. Liu, F. F. Assaad, and M. Raczkowski, *Zooming in on heavy fermions in Kondo lattice models*, *Phys. Rev. B* **104**, 155128 (2021).
- <sup>37</sup> R. Zhou, X. Zhang, and G. Li, *Doniach phase diagram for the Kondo lattice model on square and triangular lattices*, *Phys. Rev. Res.* **5**, L032014 (2023).
- <sup>38</sup> A. M. Tsvelik, *Semiclassical solution of one dimensional model of Kondo insulator*, *Phys. Rev. Lett.* **72**, 1048 (1994).
- <sup>39</sup> O. Zachar, S. A. Kivelson, and V. J. Emery, *Exact Results for a 1D Kondo Lattice from Bosonization*, *Phys. Rev. Lett.* **77**, 1342 (1996).
- <sup>40</sup> H. Tsunetsugu, Y. Hatsugai, K. Ueda, and M. Sigrist, *Spin-liquid ground state of the half-filled Kondo lattice in one dimension*, *Phys. Rev. B* **46**, 3175 (1992).
- <sup>41</sup> C. C. Yu and S. R. White, *Numerical renormalization group study of the one-dimensional Kondo insulator*, *Phys. Rev. Lett.* **71**, 3866 (1993).
- <sup>42</sup> N. Shibata, T. Nishino, K. Ueda, and C. Ishii, *Spin and charge gaps in the one-dimensional Kondo-lattice model with Coulomb interaction between conduction electrons*, *Phys. Rev. B* **53**, R8828 (1996).
- <sup>43</sup> H. Tsunetsugu, M. Sigrist, and K. Ueda, *The ground-state phase diagram of the one-dimensional Kondo lattice model*, *Rev. Mod. Phys.* **69**, 809 (1997).
- <sup>44</sup> M. Kohno, *Emergence of electronic modes by doping Kondo insulators in the Kondo lattice and periodic Anderson models*, *Phys. Rev. B* **105**, 155134 (2022).
- <sup>45</sup> M. Kohno, *Temperature-driven change in band structure reflecting spin-charge separation of Mott and Kondo insulators*, *Phys. Rev. B* **108**, 195116 (2023).
- <sup>46</sup> R. Peters and R. Rausch, *Low-energy excitations and transport functions of the one-dimensional Kondo insulator*, *SciPost Phys.* **14**, 166 (2023).
- <sup>47</sup> M. Sentef, J. Kuneš, P. Werner, and A. P. Kampf, *Correlations in a band insulator*, *Phys. Rev. B* **80**, 155116 (2009).
- <sup>48</sup> Y. Mou, R. Mondaini, and R. T. Scalettar, *Bilayer Hubbard model: Analysis based on the fermionic sign problem*, *Phys. Rev. B* **106**, 125116 (2022).
- <sup>49</sup> J. Chen, E. M. Stoudenmire, Y. Komijani, and P. Coleman, *Matrix Product Study of Spin Fractionalization in the 1D Kondo Insulator*, [arXiv:2302.09701](https://arxiv.org/abs/2302.09701) (2023).
- <sup>50</sup> E. Huecker and Y. Komijani, *Spin fractionalization in a Kondo-lattice superconductor heterostructure*, *Phys. Rev. B* **108**, 195120 (2023).
- <sup>51</sup> M. Yamanaka, M. Oshikawa, and I. Affleck, *Nonperturbative Approach to Luttinger's Theorem in One Dimension*, *Phys. Rev. Lett.* **79**, 1110 (1997).
- <sup>52</sup> S. Moukouri and L. G. Caron, *Ground-state properties of the one-dimensional Kondo lattice at partial band filling*, *Phys. Rev. B* **52**, R15723 (1995).
- <sup>53</sup> S. Moukouri and L. G. Caron, *Fermi surface of the one-dimensional Kondo-lattice model*, *Phys. Rev. B* **54**, 12212 (1996).
- <sup>54</sup> N. Shibata, K. Ueda, T. Nishino, and C. Ishii, *Friedel oscillations in the one-dimensional Kondo lattice model*, *Phys. Rev. B* **54**, 13495 (1996).
- <sup>55</sup> N. Shibata, A. Tsvelik, and K. Ueda, *One-dimensional Kondo lattice model as a Tomonaga-Luttinger liquid*, *Phys. Rev. B* **56**, 330 (1997).
- <sup>56</sup> J. C. Xavier, E. Novais, and E. Miranda, *Small Fermi surface in the one-dimensional Kondo lattice model*, *Phys. Rev. B* **65**, 214406 (2002).
- <sup>57</sup> N. Xie and Y.-f. Yang, *Interplay of localized and itinerant behavior in the one-dimensional Kondo-Heisenberg model*, *Phys. Rev. B* **91**, 195116 (2015).
- <sup>58</sup> N. Xie, D. Hu, and Y.-f. Yang, *Hybridization oscillation in the one-dimensional Kondo-Heisenberg model with Kondo holes*, *Sci. Rep.* **7**, 11924 (2017).
- <sup>59</sup> I. Khait, P. Azaria, C. Hubig, U. Schollwöck, and A. Auerbach, *Doped Kondo chain, a heavy Luttinger liquid*, *Proc. Natl. Acad. Sci. U.S.A.* **115**, 5140 (2018).
- <sup>60</sup> A. Nikolaenko and Y.-H. Zhang, *Numerical signatures of ultra-local criticality in a one dimensional Kondo lattice model*, [arXiv:2306.09402](https://arxiv.org/abs/2306.09402) (2023).
- <sup>61</sup> B. H. Bernhard, B. Coqblin, and C. Lacroix, *Frustration in the Kondo lattice model: Local versus extended singlet phases*, *Phys. Rev. B* **83**, 214427 (2011).
- <sup>62</sup> J. H. Pixley, R. Yu, and Q. Si, *Quantum Phases of the Shastry-Sutherland Kondo Lattice: Implications for the Global Phase Diagram of Heavy-Fermion Metals*, *Phys. Rev. Lett.* **113**, 176402 (2014).
- <sup>63</sup> L. Isaev and A. M. Rey, *Heavy-Fermion Valence-Bond Liquids in Ultracold Atoms: Cooperation of the Kondo Effect and Geometric Frustration*, *Phys. Rev. Lett.* **115**, 165302 (2015).
- <sup>64</sup> H. Li, H.-F. Song, and Y. Liu, *Phase diagram of the Kondo-Heisenberg model on honeycomb lattice with geometrical frustration*, *Europhys. Lett.* **116**, 37005 (2016).
- <sup>65</sup> L. Su and P. Sengupta, *Dimer-induced heavy-fermion superconductivity in the Shastry-Sutherland Kondo lattice model*, *Phys. Rev. B* **92**, 165431 (2015).
- <sup>66</sup> J. H. Pixley, R. Yu, S. Paschen, and Q. Si, *Global phase diagram and momentum distribution of single-particle excitations in Kondo insulators*, *Phys. Rev. B* **98**, 085110 (2018).



- <sup>67</sup> P. Coleman and A. H. Nevidomskyy, *Frustration and the Kondo Effect in Heavy Fermion Materials*, *J. Low Temp. Phys.* **161**, 182 (2010).
- <sup>68</sup> S. R. White and I. Affleck, *Dimerization and incommensurate spiral spin correlations in the zigzag spin chain: Analogies to the Kondo lattice*, *Phys. Rev. B* **54**, 9862 (1996).
- <sup>69</sup> M. Peschke, R. Rausch, and M. Potthoff, *Frustrated quantum magnetism in the Kondo lattice on the zigzag ladder*, *Phys. Rev. B* **97**, 115124 (2018).
- <sup>70</sup> M. Peschke, L.-M. Woelk, and M. Potthoff, *Phase diagram of the Kondo model on the zigzag ladder*, *Phys. Rev. B* **99**, 085140 (2019).
- <sup>71</sup> C. K. Majumdar and D. K. Ghosh, *On Next-Nearest-Neighbor Interaction in Linear Chain. I*, *J. Math. Phys.* **10**, 1388 (1969).
- <sup>72</sup> F. D. M. Haldane, *Spontaneous dimerization in the  $S = \frac{1}{2}$  Heisenberg antiferromagnetic chain with competing interactions*, *Phys. Rev. B* **25**, 4925 (1982).
- <sup>73</sup> E. Eidelstein, S. Moukouri, and A. Schiller, *Quantum phase transitions, frustration, and the Fermi surface in the Kondo lattice model*, *Phys. Rev. B* **84**, 014413 (2011).
- <sup>74</sup> A. Dobry, A. Jaefari, and E. Fradkin, *Inhomogeneous superconducting phases in the frustrated Kondo-Heisenberg chain*, *Phys. Rev. B* **87**, 245102 (2013).
- <sup>75</sup> J. Chen, J. Wang, and Y.-f. Yang, *Pair density wave, unconventional superconductivity, and non-Fermi liquid quantum critical phase in a frustrated Kondo lattice*, *Phys. Rev. B* **109**, 014103 (2024).
- <sup>76</sup> A. Paramekanti and J. B. Marston, *SU(N) quantum spin models: a variational wavefunction study*, *J. Phys.: Condens. Matter* **19**, 125215 (2007).
- <sup>77</sup> F. H. Kim, F. F. Assaad, K. Penc, and F. Mila, *Dimensional crossover in the SU(4) Heisenberg model in the six-dimensional antisymmetric self-conjugate representation revealed by quantum Monte Carlo and linear flavor-wave theory*, *Phys. Rev. B* **100**, 085103 (2019).
- <sup>78</sup> R. Moessner, S. L. Sondhi, and E. Fradkin, *Short-ranged resonating valence bond physics, quantum dimer models, and ising gauge theories*, *Phys. Rev. B* **65**, 024504 (2001).
- <sup>79</sup> J. C. Xavier, R. G. Pereira, E. Miranda, and I. Affleck, *Dimerization Induced by the RKKY Interaction*, *Phys. Rev. Lett.* **90**, 247204 (2003).
- <sup>80</sup> J. C. Xavier and E. Miranda, *One-dimensional Kondo lattice model at quarter filling*, *Phys. Rev. B* **78**, 144406 (2008).
- <sup>81</sup> Y. Huang, D. N. Sheng, and C. S. Ting, *Coupled dimer and bond-order-wave order in the quarter-filled one-dimensional Kondo lattice model*, *Phys. Rev. B* **102**, 245143 (2020).
- <sup>82</sup> S. Taie, E. Ibarra-Garcia-Padilla, N. Nishizawa, Y. Takasu, Y. Kuno, H.-T. Wei, R. T. Scalettar, K. R. A. Hazzard, and Y. Takahashi, *Observation of antiferromagnetic correlations in an ultracold SU(N) Hubbard model*, *Nat. Phys.* **18**, 1356 (2022).
- <sup>83</sup> A. V. Gorshkov, M. Hermele, V. Gurarie, C. Xu, P. S. Julienne, J. Ye, P. Zoller, E. Demler, M. D. Lukin, and A. M. Rey, *Two-orbital SU(N) magnetism with ultracold alkaline-earth atoms*, *Nat. Phys.* **6**, 289 (2010).
- <sup>84</sup> X. Zhang, M. Bishof, S. L. Bromley, C. V. Kraus, M. S. Safronova, P. Zoller, A. M. Rey, and J. Ye, *Spectroscopic observation of SU(N)-symmetric interactions in Sr orbital magnetism*, *Science* **345**, 1467 (2014).
- <sup>85</sup> F. Scazza, C. Hofrichter, M. Höfer, P. C. De Groot, I. Bloch, and S. Fölling, *Observation of two-orbital spin-exchange interactions with ultracold SU(N)-symmetric fermions*, *Nat. Phys.* **10**, 779 (2014).
- <sup>86</sup> L. Riegger, N. Darkwah Oppong, M. Höfer, D. R. Fernandes, I. Bloch, and S. Fölling, *Localized Magnetic Moments with Tunable Spin Exchange in a Gas of Ultracold Fermions*, *Phys. Rev. Lett.* **120**, 143601 (2018).
- <sup>87</sup> L. Wang, Z. Fu, J. Sun, M. Liu, W. Yi, C. Yi, Y. Luo, Y. Dai, G. Liu, Y. Matsushita, K. Yamaura, L. Lu, J.-G. Cheng, Y.-f. Yang, Y. Shi, and J. Luo, *Heavy fermion behavior in the quasi-one-dimensional Kondo lattice CeCo<sub>2</sub>Ga<sub>8</sub>*, *Npj Quantum Mater.* **2**, 36 (2017).
- <sup>88</sup> K. Cheng, L. Wang, Y. Xu, F. Yang, H. Zhu, J. Ke, X. Lu, Z. Xia, J. Wang, Y. Shi, Y. Yang, and Y. Luo, *Realization of Kondo chain in CeCo<sub>2</sub>Ga<sub>8</sub>*, *Phys. Rev. Mater.* **3**, 021402 (2019).
- <sup>89</sup> P. Zheng, C. Wang, Y. Xu, L. Wang, W. Wu, Y. G. Shi, Y.-f. Yang, and J. L. Luo, *Uniaxial hybridization in the quasi-one-dimensional Kondo lattice CeCo<sub>2</sub>Ga<sub>8</sub>*, *Phys. Rev. B* **105**, 035112 (2022).
- <sup>90</sup> A. E. Sikkema, I. Affleck, and S. R. White, *Spin Gap in a Doped Kondo Chain*, *Phys. Rev. Lett.* **79**, 929 (1997).
- <sup>91</sup> O. Zachar and A. M. Tsvelik, *One-dimensional electron gas interacting with a Heisenberg spin-1/2 chain*, *Phys. Rev. B* **64**, 033103 (2001).
- <sup>92</sup> E. Berg, E. Fradkin, and S. A. Kivelson, *Pair-Density-Wave Correlations in the Kondo-Heisenberg Model*, *Phys. Rev. Lett.* **105**, 146403 (2010).
- <sup>93</sup> A. M. Tsvelik, *Fractionalized Fermi liquid in a Kondo-Heisenberg model*, *Phys. Rev. B* **94**, 165114 (2016).
- <sup>94</sup> J. May-Mann, R. Levy, R. Soto-Garrido, G. Y. Cho, B. K. Clark, and E. Fradkin, *Topology and the one-dimensional Kondo-Heisenberg model*, *Phys. Rev. B* **101**, 165133 (2020).
- <sup>95</sup> R. Masui and K. Totsuka, *Electric and magnetic properties of higher-spin Kondo-Heisenberg models at strong coupling*, *Phys. Rev. B* **106**, 014411 (2022).
- <sup>96</sup> T. Hazra and P. Coleman, *Luttinger sum rules and spin fractionalization in the SU(N) Kondo lattice*, *Phys. Rev. Research* **3**, 033284 (2021).
- <sup>97</sup> K. Totsuka, *Ferromagnetism in the SU(N) Kondo lattice model: SU(N) double exchange and supersymmetry*, *Phys. Rev. A* **107**, 033317 (2023).
- <sup>98</sup> J. W. Negele and H. Orland, *Quantum Many-particle Systems* (Westview Press, Boulder, CO, 1998).
- <sup>99</sup> N. Read and D. M. Newns, *On the solution of the Coqblin-Schrieffer Hamiltonian by the large-N expansion technique*, *J. Phys. C* **16**, 3273 (1983).
- <sup>100</sup> A. Auerbach and K. Levin, *Kondo Bosons and the Kondo Lattice: Microscopic Basis for the Heavy Fermi Liquid*, *Phys. Rev. Lett.* **57**, 877 (1986).
- <sup>101</sup> S. Saremi and P. A. Lee, *Quantum critical point in the Kondo-Heisenberg model on the honeycomb lattice*, *Phys. Rev. B* **75**, 165110 (2007).
- <sup>102</sup> E. Fradkin and S. H. Shenker, *Phase diagrams of lattice gauge theories with Higgs fields*, *Phys. Rev. D* **19**, 3682 (1979).
- <sup>103</sup> S. Burdin, A. Georges, and D. R. Grempel, *Coherence Scale of the Kondo Lattice*, *Phys. Rev. Lett.* **85**, 1048 (2000).
- <sup>104</sup> D. K. Morr, *Theory of scanning tunneling spectroscopy: from Kondo impurities to heavy fermion materials*, *Rep. Prog. Phys.* **80**, 014502 (2017).

- <sup>105</sup> T. A. Costi, *Kondo Effect in a Magnetic Field and the Magnetoresistivity of Kondo Alloys*, *Phys. Rev. Lett.* **85**, 1504 (2000).
- <sup>106</sup> M. Maltseva, M. Dzero, and P. Coleman, *Electron Cotunneling into a Kondo Lattice*, *Phys. Rev. Lett.* **103**, 206402 (2009).
- <sup>107</sup> L. Borda, L. Fritz, N. Andrei, and G. Zaránd, *Theory of inelastic scattering from quantum impurities*, *Phys. Rev. B* **75**, 235112 (2007).
- <sup>108</sup> R. Blankenbecler, D. J. Scalapino, and R. L. Sugar, *Monte Carlo calculations of coupled boson-fermion systems. I*, *Phys. Rev. D* **24**, 2278 (1981).
- <sup>109</sup> S. Sorella, S. Baroni, R. Car, and M. Parrinello, *A Novel Technique for the Simulation of Interacting Fermion Systems*, *Europhys. Lett.* **8**, 663 (1989).
- <sup>110</sup> F. F. Assaad and H. Evertz, in *Computational Many-Particle Physics*, Lecture Notes in Physics, Vol. 739, edited by H. Fehske, R. Schneider, and A. Weiße (Springer, Berlin, 2008) pp. 277–356.
- <sup>111</sup> C. Wu and S.-C. Zhang, *Sufficient condition for absence of the sign problem in the fermionic quantum Monte Carlo algorithm*, *Phys. Rev. B* **71**, 155115 (2005).
- <sup>112</sup> F. F. Assaad, M. Bercx, F. Goth, A. Götz, J. S. Hofmann, E. Huffman, Z. Liu, F. P. Toldin, J. S. E. Portela, and J. Schwab, *The ALF (Algorithms for Lattice Fermions) project release 2.0. Documentation for the auxiliary-field quantum Monte Carlo code*, *SciPost Phys. Codebases*, **1** (2022).
- <sup>113</sup> A. W. Sandvik, *Stochastic method for analytic continuation of quantum Monte Carlo data*, *Phys. Rev. B* **57**, 10287 (1998).
- <sup>114</sup> K. S. D. Beach, *Identifying the maximum entropy method as a special limit of stochastic analytic continuation*, [arXiv:cond-mat/0403055](https://arxiv.org/abs/cond-mat/0403055) (2004).
- <sup>115</sup> I. Affleck and J. B. Marston, *Large- $n$  limit of the Heisenberg-Hubbard model: Implications for high- $T_c$  superconductors*, *Phys. Rev. B* **37**, 3774 (1988).
- <sup>116</sup> J. B. Marston and I. Affleck, *Large- $n$  limit of the Hubbard-Heisenberg model*, *Phys. Rev. B* **39**, 11538 (1989).
- <sup>117</sup> M. Raczkowski and F. F. Assaad, *Spinon confinement: Dynamics of weakly coupled Hubbard chains*, *Phys. Rev. B* **88**, 085120 (2013).
- <sup>118</sup> E. M. Pärshcke, Y. Wang, B. Moritz, T. P. Devereaux, C.-C. Chen, and K. Wohlfeld, *Numerical investigation of spin excitations in a doped spin chain*, *Phys. Rev. B* **99**, 205102 (2019).
- <sup>119</sup> I. Affleck and F. D. M. Haldane, *Critical theory of quantum spin chains*, *Phys. Rev. B* **36**, 5291 (1987).
- <sup>120</sup> S. Caracciolo, R. G. Edwards, A. Pelissetto, and A. D. Sokal, *Wolff-type embedding algorithms for general nonlinear  $\sigma$ -models*, *Nucl. Phys. B* **403**, 475 (1993).
- <sup>121</sup> J. des Cloizeaux and J. J. Pearson, *Spin-Wave Spectrum of the Antiferromagnetic Linear Chain*, *Phys. Rev.* **128**, 2131 (1962).
- <sup>122</sup> B. Lake, D. A. Tennant, J.-S. Caux, T. Barthel, U. Schollwöck, S. E. Nagler, and C. D. Frost, *Multispinon Continua at Zero and Finite Temperature in a Near-Ideal Heisenberg Chain*, *Phys. Rev. Lett.* **111**, 137205 (2013).
- <sup>123</sup> M. Mourigal, M. Enderle, A. Klöpperpieper, J.-S. Caux, A. Stunault, and H. M. Rønnow, *Fractional spinon excitations in the quantum Heisenberg antiferromagnetic chain*, *Nat. Phys.* **9**, 435 (2013).
- <sup>124</sup> C. Gröber and R. Eder, *Temperature-dependent band structure of the Kondo insulator*, *Phys. Rev. B* **57**, R12659 (1998).
- <sup>125</sup> T. Mutou, N. Shibata, and K. Ueda, *Temperature-Induced Gap Formation in Dynamic Correlation Functions of the One-Dimensional Kondo Insulator: Finite-Temperature Density-Matrix Renormalization-Group Study*, *Phys. Rev. Lett.* **81**, 4939 (1998).
- <sup>126</sup> N. Shibata and H. Tsunetsugu, *Dynamic Correlations in Doped 1D Kondo Insulator - Finite-T DMRG Study -*, *J. Phys. Soc. Jpn.* **68**, 3138 (1999).
- <sup>127</sup> M. J. Bhaseen, F. H. L. Essler, and A. Grage, *Itinerancy effects on spin correlations in one-dimensional Mott insulators*, *Phys. Rev. B* **71**, 020405 (2005).
- <sup>128</sup> A. Nocera, N. D. Patel, J. Fernandez-Baca, E. Dagotto, and G. Alvarez, *Magnetic excitation spectra of strongly correlated quasi-one-dimensional systems: Heisenberg versus Hubbard-like behavior*, *Phys. Rev. B* **94**, 205145 (2016).
- <sup>129</sup> T. Nishino and K. Ueda, *Spin- and charge-excitation gaps in the one-dimensional periodic Anderson model*, *Phys. Rev. B* **47**, 12451 (1993).
- <sup>130</sup> R. Assaraf, P. Azaria, M. Caffarel, and P. Lecheminant, *Metal-insulator transition in the one-dimensional SU( $N$ ) Hubbard model*, *Phys. Rev. B* **60**, 2299 (1999).
- <sup>131</sup> E. Szirmai and J. Sólyom, *Mott transition in the one-dimensional SU( $n$ ) Hubbard model*, *Phys. Rev. B* **71**, 205108 (2005).
- <sup>132</sup> K. Buchta, O. Legeza, E. Szirmai, and J. Sólyom, *Mott transition and dimerization in the one-dimensional SU( $n$ ) Hubbard model*, *Phys. Rev. B* **75**, 155108 (2007).
- <sup>133</sup> D. Wang, L. Wang, and C. Wu, *Slater and Mott insulating states in the SU(6) Hubbard model*, *Phys. Rev. B* **100**, 115155 (2019).
- <sup>134</sup> J.-X. Zhu, I. Martin, and A. R. Bishop, *Kondo Stripes in an Anderson-Heisenberg Model of Heavy Fermion Systems*, *Phys. Rev. Lett.* **100**, 236403 (2008).
- <sup>135</sup> R. Peters and N. Kawakami, *Competition of striped magnetic order and partial Kondo screened state in the Kondo lattice model*, *Phys. Rev. B* **96**, 115158 (2017).
- <sup>136</sup> Jülich Supercomputing Centre, *JUWELS Cluster and Booster: Exascale Pathfinder with Modular Supercomputing Architecture at Juelich Supercomputing Centre*, *J. Large-Scale Res. Facil.* **7**, A138 (2021).